HHS Public Access

Author manuscript

Circulation. Author manuscript; available in PMC 2022 July 20.

Published in final edited form as:

Circulation. 2021 July 20; 144(3): 210–228. doi:10.1161/CIRCULATIONAHA.120.049497.

Cyclin D2 overexpression enhances the efficacy of human induced pluripotent stem cell-derived cardiomyocytes for myocardial repair in a swine model of myocardial infarction

Meng Zhao, MD, PhD[1], **Yuji Nakada, PhD**[1], **Yuhua Wei, BS**[1], **Weihua Bian, PhD**[1], **Yuxin Chu, MD**[2], **Anton V Borovjagin, PhD**[1], **Min Xie, MD, PhD**[2], **Wuqiang Zhu, MD, PhD**[4], **Thanh Nguyen, PhD**[3], **Yang Zhou, PhD**[1], **Vahid Serpooshan, PhD**[5], **Gregory P. Walcott, MD**[1,2], **Jianyi Zhang, MD, PhD**[1,*]

[1]Department of Biomedical Engineering, School of Medicine and School of Engineering, the University of Alabama at Birmingham, Birmingham, AL, 35233, USA

[2]Division of Cardiology, Department of Medicine, School of Medicine and School of Engineering, the University of Alabama at Birmingham, Birmingham, AL, 35233, USA

[3]Informatics Institute, the University of Alabama at Birmingham, Birmingham, AL, 35233, USA

[4]Department of Cardiovascular Diseases, Physiology and Biomedical Engineering, Mayo Clinic Arizona, Scottsdale, AZ, 85259, USA

[5]Wallace H. Coulter Department of Biomedical Engineering, Department of Pediatrics, Emory University and Georgia Institute of Technology, Atlanta, GA, 30332, USA

Abstract

Background: Human-induced pluripotent stem cells (hiPSCs) with normal or upregulated levels of CCND2 expression were differentiated into cardiomyocytes ($CCND2^{WT}$CMs or $CCND2^{OE}$CMs, respectively) and injected into infarcted pig hearts.

Methods: Acute myocardial infarction (AMI) was induced via a 60-minute occlusion of the left-anterior descending coronary artery. Immediately after reperfusion, $CCND2^{WT}$CMs or $CCND2^{OE}$CMs (3×10^7 cells each), or an equivalent volume of the delivery vehicle was injected around the infarct border zone area.

Results: The number of the engrafted $CCND2^{OE}$CMs exceeded that of the engrafted $CCND2^{WT}$CMs from 6 to 8-fold, rising from 1 week to 4 weeks post-implantation. In contrast to the treatment with the $CCND2^{WT}$CMs or the delivery vehicle, the administration of $CCND2^{OE}$CM was associated with significantly improved left-ventricular function, as revealed by magnetic resonance imaging (MRI). This correlated with the reduction of infarct size, fibrosis, ventricular hypertrophy, CM apoptosis, and the increase of vascular density and arterial density, as per the histological analysis of the treated hearts. Expression of the cell proliferation markers (e.g.,

[*]**Corresponding Author:** Dr. Jianyi Zhang, M.D., Ph.D., 1670 University Boulevard, Volker Hall G094J, Department of Biomedical Engineering, School of Medicine and School of Engineering, University of Alabama at Birmingham, Birmingham, Alabama 35294, USA. Telephone: (205) 934-8421; Fax: (205) 934-9101; jayzhang@uab.edu.

Conflict of Interest Disclosures:
None.

Ki67, phosphorylated histone 3 [PH3] and Aurora Kinase B [Aurora B]) was also significantly upregulated in the recipient CMs from the CCND2^{OE}CM-treated than from the CCND2^{WT}CM-treated pigs. The cell proliferation rate and the hypoxia tolerance measured in cultured hiPSC-CMs were significantly greater after their treatment with exosomes isolated from the CCND2^{OE}CMs (CCND2^{OE}Exos) than from the CCND2^{WT}CMs (CCND2^{WT}Exos). As demonstrated by our study, CCND2^{OE}Exos can also promote the proliferation activity of postnatal rat and adult mouse cardiomyocytes. A bulk miRNA sequencing analysis of CCND2^{OE}Exos vs. CCND2^{WT}Exos identified 206 and 91 miRNAs that were significantly up- and down-regulated, respectively. Gene ontology (GO) enrichment analysis identified significant differences in the expression profiles of miRNAs from various functional categories and pathways, including miRNAs implicated in cell-cycle checkpoints (G2/M and G1/S transitions), or the mechanism of cytokinesis.

Conclusion: We have demonstrated that an enhanced potency of the CCND2^{OE}CMs promoted myocyte proliferation in both grafts and the recipient tissue in a large mammal acute myocardial infarction (AMI) model. These results suggest that the CCND2^{OE}CMs transplantation may be a potential therapeutic strategy for the repair of infarcted hearts.

Keywords

Cyclin D2; Human induced pluripotent stem cells; myocytes; Myocardial Infarction

INTRODUCTION

Although the management of clinical end stage congestive heart failure (CHF) has improved significantly in recent decades, the successful recovery is limited by the negligible regenerative capacity of the cardiomyocytes[1]. The molecular and cellular basis for the progressive heart failure is the result of the inability of damaged and apoptotic myocytes to be replaced. Strategies for promoting myocardial regeneration include the *in-vivo* reprogramming of resident cardiac fibroblasts into cardiomyocyte-like cells[2], transplantation of somatic stem/progenitor cell-derived cardiomyocytes (CMs)[3], and treatments aimed at recruiting endogenous progenitor cells or promoting cell-cycle activity and proliferation in endogenous CMs[4]. Studies in rodent models of myocardial injury evidence that CMs differentiated from human induced-pluripotent stem cells (hiPSCs) can diminish the extent of the cardiac scar formation and improve the functional recovery of the injured myocardium when implanted either directly or as components of an engineered cardiac-muscle patch[5, 6]. However, clinical studies of cardiac cell therapy have been less promising, primarily due to an exceptionally poor CM engraftment rate[7, 8]. Furthermore, the clinical implications of the observations made in small animals are difficult to interpret because of the profound physiological differences between rodents and humans. Therefore, studies using mammals are necessary to bridge these differences and facilitate the clinical translation of novel therapeutic strategies.

We previously demonstrated that an αMHC promoter-driven CCND2 transgene expressed in human induced pluripotent stem cell (hiPSC)-derived cardiomyocytes (CCND2^{OE}CMs) showed prominent proliferation ability both in vitro and following their transplantation into infarcted mouse hearts[9]. Thus, although the initial engraftment rate remained low, the

transplanted cells continued to divide and repopulate the infarcted region, so that four weeks after the cell administration the cardiac function improved, while the infarct size and hypertrophy were significantly reduced in mice receiving the $CCND2^{OE}$CMs, in contrast to the control mice treated with hiPSC-CMs that expressed wild-type (WT) levels of CCND2 ($CCND2^{WT}$CMs). Here, we examined whether the repair of injured ventricle by transplantation of hiPSC-MHC-CCND2-CMs can be achieved by promoting myocyte proliferation in a pig model of postinfarction LV remodeling.

MATERIALS AND METHODS

The data, analytic methods, and study materials will be/have been made available to other researchers for purposes of reproducing the results or replicating the procedure, and we will be responsible for maintaining availability. All experiments and procedures involving animals were approved by the Institutional Animal Care and Use Committee (IACUC, APN 20502) of the School of Medicine, the University of Alabama at Birmingham, and performed under the Guidelines for the Care and Use of Laboratory Animals published by the US National Institutes of Health (2011).

hiPSC Expansion and Maintenance

hiPSCs (GRiPS) were previously generated before from human cardiac fibroblasts by using a CytoTune™-iPS Reprogramming Kit (Invitrogen)[10]. The cells were expanded and subcultured as previously reported [10, 11]. In brief, frozen stock of the hiPSCs was thawed out, and the cells were seeded in a 6-well plate that had been coated with Matrigel (Corning), and cultured in mTeSR1 (STEMCELL Technologies) with daily medium changes to 80–90% confluency. hiPSCs were passaged every 3–4 days and differentiated into CMs after the third passage. For passaging, cells were dissociated by adding 0.5 mL of Accutase (STEMCELL Technologies) to each well and incubating at 37 °C for 5 minutes. Afterward, the cells were resuspended in mTeSR1 containing 5 μM Y-27632 (STEMCELL Technologies) and replated at the ratios between 1:6 and 1:18. Twenty-four hours later, the medium was replaced with mTeSR1 without Y-27632.

Generation of CCND2-overexpressing hiPSCs

The lenti-α-MHC/CCND2 plasmid was generated as previously described[9]. Briefly, a pair of oligonucleotides (forward: 5’AGAGCCACCGGTATGGAGCTGCTGTGCCACGAGGT 3 ‘, reverse: 5’CTGCAGGCGCGCCGAATTTTTTTTTTAAGTTT CACCCT 3’; Invitrogen) were used to amplify the CCND2 insert from a plasmid (Addgene # 8958) by PCR. The amplified product was digested with AscI and AgeI endonucleases, and separated by a 2% agarose gel for purification. The purified product was subcloned into a lentivirus-α-MHC (myosin heavy chain) vector (Addgene # 21230). The inserted sequence was confirmed by Sanger sequencing. The lentivirus-α-MHC/CCND2 plasmid and the MISSION lentivirus packaging mixture (Sigma-Aldrich) were co-transfected into HEK293 cells with Lipofectamine 2000 (Invitrogen). Forty-eight hours later, the virus-containing supernatant was collected, concentrated (Clontech), filtered with a 0.45-μm low protein binding membrane (Millipore), and immediately transfected into hiPSCs. Forty-eight hours after transfection, G418 (400 μg/mL) was added for 7 days, and then the cells were allowed to

grow in a standard culture medium until the colonies reached the size suitable for selection and expansion. CCND2 overexpression was verified by PCR and western blot.

hiPSC-CM differentiation and purification

hiPSCs were cultured in a 6-well plate with mTeSR1 medium replaced daily. For differentiation, the medium was replaced with RPMI 1640 medium supplemented with 2% B27 minus insulin (RB-medium; ThermoFisher Scientific) and 10 μM GSK-3β inhibitor CHIR99021 (CHIR, STEMCELL Technologies) when the cells reached 80–90% confluence (Day 0); 24 hrs later, the medium was replaced with CHIR-free RB-medium and the cells were cultured for another 48 hrs until day 3, then the medium was replaced with an RB-medium containing 10 μM of the Wnt inhibitor IWR1 (STEMCELL Technologies) for 48 hrs, until day 5. The medium was then replaced with IWR1-free RB-medium, and the cells were maintained for 48 hrs until day 7. Furthermore, the medium was replaced with RPMI/B27 medium (containing insulin) (ThermoFisher Scientific). Spontaneously and rhythmically beating CMs, usually appearing around day 7 after initiation of the differentiation protocol (Day 0), were purified via a selection on a modified glucose-free RPMI medium (Thermo Fisher Scientific) supplemented with 4 mM lactate (Sigma) and B27 for at least 5 days.

Acute Myocardial infarction (AMI) model and the treatment

Acute myocardial infarction (AMI) was induced in 2 month-old females of Yorkshire pig (18 kg, Snyder Farms, Birmingham) as described previously[12]. Briefly, the animals were anesthetized with inhaled 2% isoflurane USP (Fluriso™, VetOne®), intubated, and connected to a ventilator to maintain anesthesia. A left thoracotomy was performed in the fourth intercostal space to expose the heart. The roots of the first and second diagonal coronary arteries from the left anterior descending coronary artery were occluded for one hour before reperfusion. Immediately after reperfusion, animals were randomly distributed into three treatment groups (n=7 per group): animals in the MI+CCND2^{WT}CM and MI +CCND2^{OE}CM groups were administered 3×10^7 CCND2^{WT}CMs or CCND2^{OE}CMs, respectively (suspended in phosphate-buffered saline [PBS]), and animals in the MI+Vehicle group received an equal volume of PBS alone; treatments were injected into five sites around the infarcted area. The fourth group of animals (the Sham group, n=7) underwent all surgical procedures for MI induction except the ligation step and recovered without any experimental treatments. Body temperature, electrocardiograms (ECG), arterial blood pressure, and oxygen saturation were continuously monitored throughout all the surgical procedures. After surgery, animals received subcutaneous injections of buprenorphine SR (0.24 mg/kg, Buprenex®, Rupkitt Benckiser Pharmaceuticals Inc.) every 72 hs for up to 3 days and intramuscular injections of carprofen (4 mg/kg, Rimadyl®, Zoetis) every 24 hrs for up to 2 days for pain control.

Immunohistochemistry

Hearts were dehydrated with 30% sucrose at 4 °C, embedded in OCT compound (Fisher Scientific), snap-frozen, cut into 10-μm sections, and stored at –80°C. Before immunostaining, samples were washed with PBS + 0.1% Tween 20 (PBST) for 10 min, fixed with 4% paraformaldehyde (PFA) for 10 min at room temperature, permeabilized with

chilled acetone for 3 min, washed with PBST, and blocked with 10% donkey serum. Incubation with primary antibody was performed overnight at 4°C, and then the samples were washed 3 times with PBST, incubated for 30 minutes with fluorescently-labeled secondary antibodies (Table I in the Supplement), followed by washing and mounting with Antifade Mounting Medium containing DAPI (Vector Laboratories), and imaged with a fluorescence microscope. Five high-power fields (HPFs) per section, 6 sections per zone (the border zone [BZ] and remote zone [RZ]) in each animal's heart, and 7 animals per group were used for in-vivo assessments, while analyses for the in vitro study were performed in triplicates.

Small RNA sequencing and data analysis

Total RNA was extracted from cells by using TRIzol (Invitrogen), according to the manufacturer's instructions. Small RNA libraries were constructed using the Illumina Truseq™ Small RNA Preparation kit, according to Illumina's TruSeq™ Small RNA Sample Preparation Guide. The purified cDNA library was used for cluster generation on Illumina's Cluster Station and then sequenced on Illumina GAIIx, following the vendor's instrument operating instructions. ACGT101-miR v4.2 (LC Sciences) was used for sequencing data analysis[13, 14]. Briefly, raw reads were subjected to an in-house program, ACGT101-miR to remove adapter dimers, junk, low complexity, common RNA families (rRNA, tRNA, snRNA, snoRNA), and repeats. Subsequently, unique sequences with a length of 18–26 bases were mapped to specific species precursors in miRBase 22.0 by BLAST search to identify known miRNAs and novel 3p- and 5p- derived miRNAs. The differentially-expressed miRNAs identified based on normalized deep-sequencing counts were analyzed with R package limma (Figure XIIA and XIIB in the Supplement)[15]. Two computational target prediction algorithms (TargetScan 50 - http://www.targetscan.org/vert_50/ and Miranda 3.3a - https://bioweb.pasteur.fr/packages/pack@miRanda@3.3a) were used to identify miRNA binding sites. The data predicted by both algorithms were combined, and the overlaps were calculated. The GO terms and KEGG Pathway of these most abundant miRNAs, miRNA targets were also annotated. The microRNA-sequencing data are available in the Gene Expression Omnibus (GEO) database (http://www.ncbi.nlm.nih.gov/gds) under the accession number GSE161046.

Transfection with miRNA mimics

hiPSC-CMs were seeded at a density of 3×10^5 cells/well in 6-well plates. The synthetic hsa-miR-302b-3p (5'-UAAGUGCUUCCAUGUUUUAGU-3') and hsa-miR-373–3p (5'-GAAGUGCUUCGAUUUUGGGGUGU-3') mimics were transfected into the cells as per the manufacturer's protocol. Briefly, the miRNA mimics were reconstituted into a final 40 μM stock solution, 8 μl of which were diluted in 1 ml Opti-MEM medium and mixed with Lipofectamine RNAiMAX reagent (8 μl diluted in 1 ml Opti-MEM medium) at a 1:1 ratio and incubated at room temperature for 5 min. Then the miRNA mimic-lipid complex was added to the cell culture medium for 6 hrs, followed by replacing the supernatant with the standard medium. The cells were harvested 72 hrs later for further analysis.

Statistical Analysis

All results are reported as mean ± standard error (mean ± SEM). Statistical analyses were performed with SPSS software (version 20, Chicago, USA). Significant differences between two mean values were determined via the Student's Two-Tailed t-Test; and ANOVA or repeated ANOVA with the Tukey post hoc test were used for multiple (more than 2 groups) comparisons or repeated measurements. p-values of less than 0.05 were considered statistically significant.

RESULTS

Generation and differentiation of CCND2-transgenic hiPSCs

The hiPSCs used in this study were derived from reprogrammed human cardiac fibroblasts, which were described in our previous study[9]. Genomic stability analysis was performed in both wild type hiPSCs and CCND2-expressing transgenic hiPSCs by using a G-banding karyotyping approach, which confirmed the chromosomal integrity of the two cell lines (Figure IA and IB in the Supplement).

Differentiation of the hiPSCs to cardiomyocytes (CMs) was performed by the GiWi (GSK3 inhibitor and Wnt inhibitor) protocol[16]. After metabolic purification in a medium containing lactate, but no glucose, the purity of the final $CCND2^{WT}$CM and $CCND2^{OE}$CM populations evaluated by flow cytometry was as high as 99.1% and 98.7%, respectively (Figure IIA in the Supplement). Almost all of these hiPSC-derived cardiomyocytes (hiPSC-CMs) express cardiac-specific markers, including cTnT and NKX2.5 (Figure IIB in the Supplement). Furthermore, to verify the human origin and the identity of the implanted CMs in the infarcted porcine hearts, we performed co-staining of the heart slices at 4 weeks post-transplantation for the human nuclear antigen (HNA) and NKX2.5 markers. Our results confirmed that the cardiomyocytes account for more than 98% of the implanted cells in both treatment groups (Figure IIC in the Supplement). The human CCND2 gene was placed under the αMHC promoter control, specifically driving the transgene expression in cardiomyocytes. Selective overexpression of CCND2 was verified by qRT-PCR (Figure IIIA in the Supplement), western blot (Figure IIIC in the Supplement), and immunofluorescence analysis (Figure IIIB and IIID in the Supplement).

Implanted $CCND2^{OE}$CMs are significantly more potent than $CCND2^{WT}$CMs for myocardial recovery

AMI was surgically induced in Yorkshire female pigs via ligation of the left-anterior descending (LAD) coronary artery (Figure 1A). The animals were randomly segregated to experimental groups for treatments with: $CCND2^{OE}$CMs (i.e., the MI+$CCND2^{OE}$CMs group), $CCND2^{WT}$CMs (the MI+$CCND2^{WT}$CMs group), or with the delivery vehicle only (the MI+Vehicle only group) (Figure IVA in the Supplement). The fourth treatment group (the SHAM group) was subjected to all the surgical procedures for AMI induction, except for the LAD coronary artery ligation step, and recovered without any experimental treatments. Cardiac magnetic resonance imaging (cMRI) assessments performed 4 weeks after the AMI induction (Figure 1B), demonstrated that left ventricular (LV) ejection fraction (EF) (Figure 1C), end-diastolic volume (EDV) (Figure 1D), and end-systolic volume (ESV)

(Figure 1E) were significantly improved in the MI+CCND2^{OE}CMs animals as compared to the MI+CCND2^{WT}CMs animals, or in both cell-treatment groups relative to the MI+Vehicle control animals.

Scar sizes, whether quantified via cMRI (Figure 1F and 1H) or by histological assessments of the freshly prepared tissue sections (Figure 1G and 1I), were found significantly reduced in the MI+CCND2^{OE}CM group than in either MI+Vehicle or MI+CCND2^{WT}CM animals. In contrast, scar size measurements in Vehicle- and CCND2^{WT}CM-treated animals were similar. Furthermore, when fibrosis was assessed by quantification of Sirius Red- and Fast Green-stained tissue sections (Figure 1J and 1K), the measurements were significantly lower in MI+CCND2^{OE}CM animals than in either the MI+Vehicle or MI+CCND2^{WT}CM animals.

The graft-related arrhythmia is a primary risk associated with hiPSC-CMs therapy. Continuous ECG recordings were made from the time of infarction until the animal sacrifice by using an implantable loop recorder for porcine models. All the animals showed severe arrhythmias and ST elevations due to the ischemia-reperfusion injury, but no spontaneous arrhythmia was noted during the 4-week follow-up period. Additionally, there was no statistical difference in the incidents of ventricular tachycardia (VT) or ventricular fibrillation (VF) among the MI only-, the MI+CCND2^{WT}CM- and the MI+CCND2^{OE}CM-treated hearts in response to programmed electrical stimulation (PES), which demonstrated that their electrophysiological characteristics were not impaired by CCND2^{WT}CM or CCND2^{OE}CM transplantation.

CCND2 overexpression promotes proliferation of the transplanted hiPSC-CMs

One month after the surgery, the hearts were harvested and cross-sectioned from base to apex (Figure IVB in the Supplement). Each slice was divided into different zones, according to coronary perfusion/physiology, for histological and molecular analysis (Figure IVC in the Supplement). The cell injection zone was further divided into additional sub-regions for the target gene analyses and other studies (Figure 2A). Because human male-derived CCND2^{OE}CMs and CCND2^{WT}CMs were engrafted into female pigs, the engraftments were assessed via qRT-PCR-based quantification of the Y-chromosome levels (Figure VB in the Supplement) and identified by immunostaining of human nuclear antigen (HNA) (Figure 2B, 2C and Figure VA in the Supplement).

The engraftment rates in both cell-treatment groups were similar, when measured only one week after the cell administration. However, the number of engrafted cells in the CCND2^{OE}CM group increased in subsequent weeks and was ~7-fold higher than that in the CCND2^{WT}CM-treated animals 4 weeks post-implantation (Figure 2B, 2C and Figure VB in the Supplement). It is noteworthy that most of the transplanted hiPSC-CMs were located at the junction of the infarct area and the border zone (Figure 2B). The proportion of HNA^{+} CMs co-expressing the proliferation markers Ki67 (Figure 2D) and PH3 (Figure 2E) was also significantly greater (4- and 7-fold, respectively) at 4 weeks in the CCND2^{OE}CM-treated than in the CCND2^{WT}CM-treated hearts, whereas HNA^{+} CMs that also stained positively in TUNEL assay were equally common in both cell-treatment groups (Figure 2E). Thus the higher engraftment rates observed in CCND2^{OE}CM-treated hearts were likely to be caused by an increase in CM proliferation rather than a decrease in apoptosis.

To further verify that the proliferating cells were cardiomyocytes, we also quantified the percentage of $Ki67^{+}/NKX2.5^{+}$ (Figure VIA in the Supplement) and $PH3^{+}/NKX2.5^{+}$ (Figure VIB in the Supplement) cell populations in the grafts, and the results were consistent with those obtained by using HNA as a marker. Therefore, it was further verified that the engrafted CM proliferation played a pivotal role in the cardiac functional recovery observed after transplantation.

CCND2 overexpression in the transplanted hiPSC-CMs also promotes proliferation of the recipient (porcine) cardiomyocytes adjacent to the graft

The myocardial regions with native (recipient) CMs had undetectable levels of HNA expression in the border zone (BZ) of the hearts from both cell-treatment groups (Figure VII in the Supplement), indicating that those cells were not derived from the transplanted hiPSC-CMs or proliferation. Nevertheless, Ki67 (Figure 3A) and PH3 (Figure 3B) markers were more frequently expressed in the BZ CMs from the MI+$CCND2^{OE}$CM animals than those from the MI+$CCND2^{WT}$CM or MI+Vehicle treatment groups.

Analysis of the Aurora B expression allowed to distinguish CMs that were undergoing karyokinesis with the subsequent cytokinesis (symmetrical Aurora B [SAB]) from the ones without cytokinesis[17] (asymmetrical Aurora B [ASAB]), indicating that some recipient CMs in the $CCND2^{OE}$CM-treated hearts were truly proliferating. On the contrary, multinucleation (karyokinesis) only events were observed in the recipient CMs from the $CCND2^{WT}$CM- and the Vehicle only-treated hearts (Figure 3C). The Aurora B expression was also significantly upregulated in the BZ CMs from the MI+$CCND2^{OE}$CM animal group as compared with those from the MI+$CCND2^{WT}$CM or MI+Vehicle only animals (Figure 3C). In contrast, the expression of Ki67, PH3, and Aurora B in CMs from the remote (i.e., noninfarcted) zone (RZ) did not exhibit any significant difference among the three treatment groups.

At 4 weeks after the surgery, single CMs from the BZ of the infarcted hearts were isolated and the calculated percentage of mononuclear and binuclear CMs from the BZ of the $CCND2^{OE}$CM-treated hearts was found to be significantly higher relative to that in the $CCND2^{WT}$CM- and Vehicle only-treated hearts. In contrast, the percentage of multinucleated cardiomyocytes was relatively lower (Figure 3D).

Furthermore, there were fewer $TUNEL^{+}$ CMs in the BZ (Figure 3E), the CM cross-sectional surface area was significantly smaller, and the density of CM nuclei was significantly higher (Figure 3F) in the BZs of the hearts from both cell-treatment groups than in the hearts from the MI+Vehicle only animals, as well as in the $CCND2^{OE}$CM-treated hearts relative to the $CCND2^{WT}$CM-treated hearts.

Collectively, these observations indicated that the $CCND2^{OE}$CMs increased proliferation and survival of the recipient (native porcine) CMs as opposed to hypertrophy as a typical CM response to MI. Notably, the cross-sectional surface areas of the RZ CMs were significantly smaller in the hearts from both cell-treatment groups as compared to those from the MI+Vehicle only animals as well as in the $CCND2^{OE}$CM-treated hearts relative to the $CCND2^{WT}$CM-treated hearts (Figure 3F), which suggests that not only $CCND2^{OE}$CMs, but

to a lesser extent also CCND2^{WT}CMs were able to protect the entire left ventricle from MI-related hypertrophy.

CCND2^{OE}CMs promote angiogenesis in the border zone of myocardial infarction

VEGF plays an important role in cardiac angiogenesis following myocardial infarction (MI)[18]. VEGF receptors (VEGFR) were examined in the BZ of the infarcted porcine hearts 7 days post-MI. We found that CCND2^{OE}CMs increased the number of VEGFR positive cells compared to the vehicle only or the CCND2^{WT}CM treatment group (Figure 4A). Four weeks after the cell transplantation, the proliferation markers were found to be more frequently co-expressed with either smooth muscle actin (SMA) (Figure 4B and 4C) or with the endothelial marker isolectin B4 (Figure 4D and 4E) in the BZ cells from the CCND2^{OE}CM-treated than in those from the CCND2^{WT}CM-treated hearts. Furthermore, vessel-like structures expressing SMA or the endothelial marker CD31 were significantly more common in the BZs of hearts from both cell-treatment groups than in Vehicle only-treated animals as well as in the CCND2^{OE}CM-treated relative to the CCND2^{WT}CM-treated hearts (Figure 4F). Thus, CCND2 overexpression appears to promote a pro-angiogenic activity of the transplanted hiPSC-CMs, which is likely to contribute to at least some of the improvements in the cardiac function and engraftment observed in the MI+CCND2^{OE}CM animals[19].

Exosomes secreted by the CCND2^{OE}CMs promote proliferation and hypoxia tolerance in cultured CMs

The crucial role of exosomes as mediators of extracellular signaling, implicated in the mechanisms of cardiac recovery from myocardial injury, has been well-documented[20]. In this regard, we sought to understand whether the improvements in CM proliferation and survival associated with CCND2 overexpression in transplanted hiPSC-CMs, could be recapitulated *in vitro* via CM treatment with the exosomes secreted by the CCND2^{OE}CMs. Exosomes (Exos) isolated from the culture medium of the CCND2^{WT}CMs (CCND2^{WT}Exos) and the CCND2^{OE}CMs (CCND2^{OE}Exos) were 125 nm and 105 nm in diameter, respectively (Figure 5A and 5B). Both exosome populations expressed several exosome-specific markers, such as Alix, CD81, CD9, and TSG101 (Figure 5C). Fluorescence imaging of CCND2^{WT}CMs that had been cultured with PK26-labeled CCND2^{OE}Exos or CCND2^{WT}Exos confirmed that the cells took up the fluorescent label over a 2–12 hr period (Figure 5D). Furthermore, after three days in culture, the expression levels of Ki67 (Figure 5E and 5I), PH3 (Figure 5F and 5J), and Aurora B (Figure 5G and 5K) cell proliferation markers in the CCND2^{WT}CMs treated with CCND2^{OE}Exos became significantly higher than in the CCND2^{WT}Exo-treated cells or in the cells that received no exosome treatment at all. In addition, the CCND2^{WT}CMs were more resistant to hypoxia-induced apoptosis in vitro following treatment with CCND2^{OE}Exos than those cultured in the presence of CCND2^{WT}Exo or in the absence of exosomes (Figure 5H and 5L).

CCND2^{OE}Exos were found to be able to promote the proliferation of not only cardiomyocytes, but also human umbilical vein endothelial cells (HUVEC) and human vascular smooth muscle cells (HVSMC) in vitro, as indicated by the large number of ki67^{+} and PH3^{+} HUVECs and SMCs in the CCND2^{OE}Exos-treated group, relative to those in the

vehicle only- or CCND2^{WT}Exos-treated groups (Figure X in the Supplement). Besides, exosome treatment was also capable of reducing the number of apoptotic cells in HUVEC and SMC populations under hypoxic conditions (Figure XI in the Supplement).

We also examined the effects of the hiPSC-CM-derived exosomes on the proliferation of postnatal CMs, isolated from 7 days-old rats, in which CM proliferation was already almost undetectable[21]. Treatment of the rat postnatal CMs with CCND2^{OE}Exos led to a significant increase in the number of Ki67^{+}, PH3^{+}, and Aurora B^{+} CMs, whereas CCND2^{WT}Exos failed to induce a similar proliferation activity in the rat CMs (Figure VIIIA–VIIIC in the Supplement). These data suggest that CCND2^{OE}Exos were capable of increasing rat postnatal CM proliferation.

In yet another experiment, adult CMs were isolated from a 3 month-old mouse heart and treated with PBS, CCND2^{WT}Exos, or CCND2^{OE}Exos. Remarkably, only CCND2^{OE}Exos were able to trigger proliferation markers in the adult CMs (Figure IXA and IXB in the Supplement). Moreover, the CCND2^{OE}Exos treatment induced even a partial de-differentiation of adult CMs, evidenced by a microscopy-based visualization of poorly organized sarcomere structures in those cells (Figure IXC and IXD in the Supplement).

A comparative bulk sequence analysis of miRNAs from CCND2^{WT}Exos and CCND2^{OE}Exos was performed to discover miRNAs might be responsible for CM proliferation. The sequence analysis identified 1072 total miRNAs, 651 of which were found in both Exos types, 332 were specific to CCND2^{OE}Exos, and 89 miRNAs were found only in CCND2^{WT}Exos (Figure 6A). Out of the 651 miRNAs common for both Exos types, 206 and 91 miRNAs were significantly up- and down-regulated in CCND2^{OE}Exos, respectively (Figure 6B). Gene ontology (GO) enrichment analyses identified significant differences in miRNAs of most functional categories and signaling pathways (Figure XIII in the Supplement), including miRNAs implicated in G2/M and G1/S cell cycle transitions, cell cycle arrest and mitosis (Figure 6C), as well as in the regulation of cell death and apoptosis (Figure 6D). The cell-cycle associated miRNAs with significantly different expression levels are depicted in the heat map of Figure 6E. We found that miRNAs with the highest upregulation levels include miR302-367 and miRNA371-373 clusters, which have been demonstrated to promote cardiomyocyte proliferation[22, 23]. Their sequences are highly conserved in humans and mice, and they can activate the Hippo pathway involved in the regulation of cell proliferation and programmed cell death during organ development. The miR-302-367 cluster and miR-373 can target multiple components of the Hippo signaling pathway, including MST1, LATS2, and MOB1b, thereby dephosphorylating a downstream protein Yap and promoting its translocation to the nucleus, where it interacts with the TEAD transcription factor family members and activates expression of series of genes, including the ones that promote cell proliferation and survival[24].

We further investigated the effects of individual miR-302 or miR-373 family members on the proliferation of hiPSC-CMs. After delivering miR-302b-3p or miR-373-3p mimics into hiPSC-CMs, the number of Ki67^{+}, PH3^{+}, and Aurora B (AuB)$^{+}$ cardiomyocytes was significantly increased, and a synergistic effect was observed by co-transfecting with these two mimics (Figure 6H and 6J–6L). Furthermore, this effect could be reversed by CM

transfection with the YAP-targeting siRNA, indicating that miR-373-302b could promote CM proliferation, at least partly, via regulation of YAP. In addition, the nuclear translocation of YAP increased after the transfection of miR-373-302b mimic, and this effect could be abolished by RNA silencing with the YAP mRNA-targeting siRNA (Figure 6M). Furthermore, we observed that the treatment by miR-302b-3p and miR-373-3p mimics decreased Lats2 expression and YAP phosphorylation, suggesting that the Hippo pathway was off (Figure 6G and 6I).

The effects of miR-373-302b overexpression on postnatal cardiomyocyte proliferation

We further tested whether the identified miRNAs could stimulate the proliferation of postnatal rat CMs, isolated from a 7 days-old rat, by transfecting the CMs with miR-373-302b or Ctrl miRNA mimics. The transfection outcome was examined 48 hrs later, and it was found that the percentage of $Ki67^+$, $PH3^+$, and Aurora B^+ CMs were substantially increased in the miR-373-302b mimic-transfectants, as compared to those in the Ctrl mimic-transfected group (Figure 7A–7C). This experiment evidenced that transient overexpression of miR-373-302b can induce the proliferation of postnatal rat CMs.

In addition, a loss-of-function study was performed by using a YAP-targeting siRNA, which suggested that a direct silencing of YAP expression in rat CMs can reverse the pro-proliferative effect of the miR-373-302b overexpression, as evidenced by a significant decrease in the levels of the cell cycle markers (Figure 7A–7C). Meanwhile, immunostaining for total cellular Yap protein demonstrated an increase in Yap nuclear translocation in the miR-373-302b mimic-transfected CMs, and this effect could be reversed by the YAP mRNA-targeting siRNA (Figure 7D). Furthermore, it was reported that an increased expression of miR-302b led to the activation of adult cardiomyocyte proliferation and reduced scar formation in a mouse MI model, partly through the repression of the Hippo pathway[22].

The 3′UTR sequence of the LATS2 mRNA is highly conserved in humans and swine (Figure XIV in the Supplement), and bioinformatics analysis by Targetscan software showed that the porcine LATS2 mRNA is a potential target for both hsa-miR-302b-3p and hsa-miR-373-3p. We sought to experimentally validate the above hypothesis by using miR-302b-3p as a model and a luciferase assay in HEK293T culture cells. To this end, we constructed a vector containing the luciferase reporter gene fused to the porcine wild-type (WT) LATS2 3’UTR sequence or a mutant 3’UTR with a mismatched sequence at the predicted miR-302b-3p binding site as a targeting specificity control. After co-transfection of HEK293T cells with the WT LATS2 3’UTR plasmid and miR-302b-3p mimic, luciferase activity in the transfectants was significantly reduced, as compared to the cells co-transfected with Ctrl mimic or the mutant 3’UTR-containing control construct (MUT), which indicates that the porcine LATS2 mRNA is a direct target of hsa-miR-302b-3p (Figure 7F).

To determine whether the transplanted $CCND2^{OE}$CMs can induce native porcine CM proliferation by regulating Hippo signaling, we examined the nuclear translocation of YAP in CMs of the infarct BZ of the infarcted porcine hearts. Immunostaining of the $CCND2^{OE}$CMs-treated hearts for the total intracellular Yap revealed an increase in the

nuclei-localized protein, in contrast to the vehicle only-treated or CCND2^{WT}CMs-treated hearts (Figure 7E). These results suggest that the exosomes secreted from the transplanted CCND2^{OE}CMs might deliver miR-302b-3p and miR-373-3p to the border zone and promote cardiomyocyte proliferation through inhibition of the Hippo pathway (Figure 7G).

DISCUSSION

We have previously demonstrated that the human CCND2 overexpression in hiPSCs can constitutively activate the cell cycle of hiPSC-CMs prior to their differentiation into cardiomyocytes. Intramyocardially-injected CCND2^{OE}CMs can promote the remuscularization of the infarcted immuno-deficient mouse hearts, which attenuates LV remodeling and reduces cardiac dysfunction[9]. However, the clinical relevance of using rodent models is limited by significant physiological differences between rodent and human hearts regarding size and electrical conduction as well as the formation and distribution of collateral coronary arteries[25]. Thus, large-animal research models, particularly porcine-based models, are important for developing and characterizing novel therapeutic approaches, their efficacy and safety, as well as for optimizing the dose, frequency, and routes of administration.

The data presented in this report are the results of the first study to demonstrate that overexpression of the human CCND2 can induce a significant proliferative activity (cell cycle activation) in transplanted cardiomyocytes also in a large animal model of AMI, which has the higher clinical relevance to the human disease.

CCND2^{OE}CMs injected into the injured porcine hearts were associated with significantly improved characteristics of the LV function as well as reduced heart fibrosis and hypertrophy 4 weeks post-injury/treatment, as opposed to CCND2^{WT}CMs exhibiting wild type levels of CCND2.

The reduction of fibrotic scar size occurred primarily due to a robust proliferation of the engrafted CCND2^{OE}CMs, which increased their number from 6 to 8 times relative to that of the implanted CCND2^{WT}CMs. Notably, the enhanced proliferative capability of CCND2^{OE}CMs allowed lowering of the initial administration dose of the CMs down to 3×10^7, making it an order of magnitude smaller than the dose of the human embryonic stem cell-derived CMs (1.0×10^9 and 7.5×10^8) used for transplantation into infarcted primate hearts in two previous reports[26, 27]. This difference may partially explain why we found no evidence of arrhythmogenic complications associated with the therapeutic cell administration in the aforementioned primate studies. We also observed an increase in the expression of proliferative markers (e.g., Ki67, PH3) in various types of the recipient cardiac cells (CMs, ECs, and SMCs) from the CCND2^{OE}CM-treated hearts, which is consistent with the robust paracrine activity observed in other investigations with transplanted stem-cell-derived CMs[28]. hiPSC-CMs and rodent cardiomyocytes exhibited higher proliferative activity upon co-culture with the Exosome released from the CCND2^{OE} or miR-373-302b mimic.

Cardiac fibrosis directly causes systolic and diastolic dysfunction by stiffening the myocardium[29], whereas perivascular fibrosis of the coronary arteries and arterioles[30] reduces oxygen and nutrient supply to the myocardium. The capillary network is unable to support sustained cardiac overload[31]. Thus, even after recovering from the initial infarct event, fibrosis can continue affecting the viability of the BZ cardiomyocytes through the disintegration of the extracellular matrix and replacement of the necrotic myocardial tissue by an expanding scar[32, 33]. Remarkably, the CCND2^{OE}CM transplantation promoted survival of the native or recipient CMs and also significantly increased proliferation of both recipient CMs and vascular cells, while BZ vascular density was significantly increased in the CCND2^{OE}CM-treated relative to the CCND2^{WT}CM-treated animals. This enhancement of the angiogenic response to AMI is likely to contribute to the improved myocardial performance associated with the CCND2^{OE}CM implantation, owing to the enhanced myocardial perfusion preserving[34], the reduced hypertrophy[35], and the reduced accumulation of immature collagen fibers[31]. It also facilitated the cross-talk between coronary ECs and CMs that improves myocardial functionality[36]. Although the role of cytokines, such as vascular endothelial growth factor (VEGF) and angiopoietin-1[19], in the pro-angiogenic and cytoprotective activities of various cell populations has been well-established, it is yet to be understood whether and to what extent these factors contribute to the pro-angiogenic activity of the transplanted CCND2^{OE}CMs.

The well-documented role of exosomes in cell-to-cell communication[37] and paracrine activity of the transplanted cells[38] was further supported by our observations that hiPSC-CMs, postnatal rat CMs, and adult mouse CMs exhibited higher proliferative activity upon their co-culturing in the presence of CCND2^{OE}Exos than following their treatment with CCND2^{WT}Exos, while CCND2^{OE}Exos exhibited an ability to protect cultured hiPSC-CMs from hypoxia-induced apoptosis. Notably, the miRNA profiles of CCND2^{OE}Exos and CCND2^{WT}Exos were found to be dramatically different from each other, particularly with regard to miRNAs implicated in the regulation of cell proliferation and apoptosis. The miRNA profile specific to CCND2^{OE}Exos appears to agree with the data from previous studies: miRNAs are known to promote cell proliferation and/or suppress apoptosis (e.g., miR-371-373 cluster[23], miR302-367 cluster[9, 22]) were abundant/upregulated. In contrast, those implicated in suppressing cell proliferation and/or promoting apoptosis (e.g., miR-143-3p[39], miR-506-3p[40]) were underrepresented/down-regulated. We further demonstrated that miR-302b-3p and miR-373-3p were able to promote the proliferation of hiPSC-CM and postnatal rat CMs, at least partly through regulating the HIPPO signal transduction pathway. Since the 3’UTR sequences of the LATS2 mRNAs in swine and humans are highly homologous (Figure XIV in the Supplement), we reasoned that miR-302b-3p and miR-373-3p are likely to play the same functional roles also in porcine cardiomyocytes. This hypothesis was confirmed in our study by a dual-luciferase reporter assay, demonstrating that the porcine LATS2 mRNA is also a direct target of hsa-miR-302b-3p (Figure 7F). In addition, the CCND2^{OE}CM-treated hearts showed a significant increase in the number of nuclear-Yap+ cardiomyocytes. These data demonstrate the HIPPO-YAP signaling regulation could play an important role in activating the proliferative activity of recipient cardiomyocytes of pig hearts.

Previous reports and our current study have generally focused on molecules involved in regulating the cell-cycle (e.g., cyclins and cyclin-dependent kinases) or tumor suppression[21, 41]. The most recent studies have linked a number of miRNAs to the regulation of CM proliferation and/or cardiac repair in mice and swine[42, 43]. Thus, as the therapeutic potential of exosomes for improving cardiac function becomes more evident, combining an exosome-mediated delivery of proliferative miRNAs with transplantation of CCND2^{OE}CMs (or other genetically modified cells) could become a new promising strategy for upregulating proliferation of the recipient CMs and reducing cardiac fibrosis.

In conclusion, the results presented in this report demonstrate the enhanced potency of the CCND2-overexpressing hiPSC-CMs in repairing of AMI hearts in the context of a large-animal model. CCND2^{OE}CMs can proliferate and increase in numbers from week 1 to week 4 after transplantation into the infarcted pig hearts, and the measured parameters of the cardiac performance, fibrosis, and hypertrophy resulting from the treatment, suggest significant improvements in the hearts grafted with the CCND2^{OE}CMs rather than CCND2^{WT}CMs. Importantly, the CCND2^{OE}CM transplantation was also capable of promoting the proliferation of recipient CMs, ECs, and SMCs, while no treatment-related arrhythmogenic complications were noted. Altogether, our data suggest that cardiac cell therapy involving CMs with enhanced proliferation capacity, may become an efficacious future strategy for myocardial repair and prevent CHF in patients with AMI.

Supplementary Material

Refer to Web version on PubMed Central for supplementary material.

Acknowledgments:

We thank the UAB Flow Cytometry and Single Cell Core, and the UAB Genomics Core.

Sources of Funding:

This study is supported in part by the US National Institutes of Health National Heart, Lung, and Blood Institute grants RO1 HL114120, HL131017, HL149137, and UO1 HL134764.

Non-standard Abbreviations and Acronyms:

hiPSCs
human induced pluripotent stem cells

hiPSC-CMs
human induced pluripotent stem cells-derived cardiomyocytes

CCND2^{OE}CMs or CCND2^{WT}CMs
overexpressed or wild type expressed CCND2 under control of the Myosin Heavy Chain (MHC) promoter and differentiated into cardiomyocytes

AMI
Acute myocardial infarction

HUVEC
human umbilical vein endothelial cells

HVSMC
human vascular smooth muscle cells

SMA
smooth muscle actin

SAB
symmetrical Aurora B

ASAB
asymmetrical Aurora B

REFERENCES

1. Ingason AB, Goldstone AB, Paulsen MJ, Thakore AD, Truong VN, Edwards BB, Eskandari A, Bollig T, Steele AN and Woo YJ. Angiogenesis precedes cardiomyocyte migration in regenerating mammalian hearts. J Thorac Cardiovasc Surg. 2018;155:1118–1127 e1. [PubMed: 29452461]
2. Qian L, Huang Y, Spencer CI, Foley A, Vedantham V, Liu L, Conway SJ, Fu JD and Srivastava D. In vivo reprogramming of murine cardiac fibroblasts into induced cardiomyocytes. Nature. 2012;485:593–8. [PubMed: 22522929]
3. Quevedo HC, Hatzistergos KE, Oskouei BN, Feigenbaum GS, Rodriguez JE, Valdes D, Pattany PM, Zambrano JP, Hu Q, McNiece I, Heldman AW and Hare JM. Allogeneic mesenchymal stem cells restore cardiac function in chronic ischemic cardiomyopathy via trilineage differentiating capacity. Proc Natl Acad Sci U S A. 2009;106:14022–7. [PubMed: 19666564]
4. Tao G, Kahr PC, Morikawa Y, Zhang M, Rahmani M, Heallen TR, Li L, Sun Z, Olson EN, Amendt BA and Martin JF. Pitx2 promotes heart repair by activating the antioxidant response after cardiac injury. Nature. 2016;534:119–23. [PubMed: 27251288]
5. Lou X, Zhao M, Fan C, Fast VG, Valarmathi MT, Zhu W and Zhang J. N-cadherin overexpression enhances the reparative potency of human-induced pluripotent stem cell-derived cardiac myocytes in infarcted mouse hearts. Cardiovasc Res. 2020;116:671–685. [PubMed: 31350544]
6. Wang Q, Yang H, Bai A, Jiang W, Li X, Wang X, Mao Y, Lu C, Qian R, Guo F, Ding T, Chen H, Chen S, Zhang J, Liu C and Sun N. Functional engineered human cardiac patches prepared from nature's platform improve heart function after acute myocardial infarction. Biomaterials. 2016;105:52–65. [PubMed: 27509303]
7. Zeng L, Hu Q, Wang X, Mansoor A, Lee J, Feygin J, Zhang G, Suntharalingam P, Boozer S, Mhashilkar A, Panetta CJ, Swingen C, Deans R, From AH, Bache RJ, Verfaillie CM and Zhang J. Bioenergetic and functional consequences of bone marrow-derived multipotent progenitor cell transplantation in hearts with postinfarction left ventricular remodeling. Circulation. 2007;115:1866–75. [PubMed: 17389266]
8. Ye L, Chang YH, Xiong Q, Zhang P, Zhang L, Somasundaram P, Lepley M, Swingen C, Su L, Wendel JS, Guo J, Jang A, Rosenbush D, Greder L, Dutton JR, Zhang J, Kamp TJ, Kaufman DS, Ge Y and Zhang J. Cardiac repair in a porcine model of acute myocardial infarction with human induced pluripotent stem cell-derived cardiovascular cells. Cell Stem Cell. 2014;15:750–61. [PubMed: 25479750]
9. Zhu W, Zhao M, Mattapally S, Chen S and Zhang J. CCND2 Overexpression Enhances the Regenerative Potency of Human Induced Pluripotent Stem Cell-Derived Cardiomyocytes: Remuscularization of Injured Ventricle. Circulation research. 2018;122:88–96. [PubMed: 29018036]
10. Zhang L, Guo J, Zhang P, Xiong Q, Wu SC, Xia L, Roy SS, Tolar J, O'Connell TD, Kyba M, Liao K and Zhang J. Derivation and high engraftment of patient-specific cardiomyocyte sheet using

induced pluripotent stem cells generated from adult cardiac fibroblast. Circ Heart Fail. 2015;8:156–66. [PubMed: 25420485]

11. Zhao M, Tang Y, Ernst PJ, Kahn-Krell A, Fan C, Pretorius D, Zhu H, Lou X, Zhou L, Zhang J and Zhu W. Enhancing the Engraftment of Human Induced Pluripotent Stem Cell-derived Cardiomyocytes via a Transient Inhibition of Rho Kinase Activity. J Vis Exp. 2019;149. DOI:10.3791/59452
12. Xiong Q, Ye L, Zhang P, Lepley M, Swingen C, Zhang L, Kaufman DS and Zhang J. Bioenergetic and functional consequences of cellular therapy: activation of endogenous cardiovascular progenitor cells. Circ Res. 2012;111:455–68. [PubMed: 22723295]
13. Li M, Xia Y, Gu Y, Zhang K, Lang Q, Chen L, Guan J, Luo Z, Chen H, Li Y, Li Q, Li X, Jiang AA, Shuai S, Wang J, Zhu Q, Zhou X, Gao X and Li X. MicroRNAome of porcine pre- and postnatal development. PLoS One. 2010;5:e11541.
14. Wei Z, Liu X, Feng T and Chang Y. Novel and conserved micrornas in Dalian purple urchin (Strongylocentrotus nudus) identified by next generation sequencing. Int J Biol Sci. 2011;7:180–92. [PubMed: 21383954]
15. Ritchie ME, Phipson B, Wu D, Hu Y, Law CW, Shi W and Smyth GK. limma powers differential expression analyses for RNA-sequencing and microarray studies. Nucleic Acids Res. 2015;43:e47. [PubMed: 25605792]
16. Zhao M, Tang Y, Zhou Y and Zhang J. Deciphering Role of Wnt Signalling in Cardiac Mesoderm and Cardiomyocyte Differentiation from Human iPSCs: Four-dimensional control of Wnt pathway for hiPSC-CMs differentiation. Sci Rep. 2019;9:19389. [PubMed: 31852937]
17. Hesse M, Doengi M, Becker A, Kimura K, Voeltz N, Stein V and Fleischmann BK. Midbody Positioning and Distance Between Daughter Nuclei Enable Unequivocal Identification of Cardiomyocyte Cell Division in Mice. Circ Res. 2018;123:1039–1052. [PubMed: 30355161]
18. Lv YX, Zhong S, Tang H, Luo B, Chen SJ, Chen L, Zheng F, Zhang L, Wang L, Li XY, Yan YW, Pan YM, Jiang M, Zhang YE, Wang L, Yang JY, Guo LY, Chen SY, Wang JN and Tang JM. VEGF-A and VEGF-B Coordinate the Arteriogenesis to Repair the Infarcted Heart with Vagus Nerve Stimulation. Cell Physiol Biochem. 2018;48:433–449. [PubMed: 30016789]
19. Tao Z, Chen B, Tan X, Zhao Y, Wang L, Zhu T, Cao K, Yang Z, Kan YW and Su H. Coexpression of VEGF and angiopoietin-1 promotes angiogenesis and cardiomyocyte proliferation reduces apoptosis in porcine myocardial infarction (MI) heart. Proc Natl Acad Sci U S A. 2011;108:2064–9. [PubMed: 21245320]
20. Kanada M, Bachmann MH, Hardy JW, Frimannson DO, Bronsart L, Wang A, Sylvester MD, Schmidt TL, Kaspar RL, Butte MJ, Matin AC and Contag CH. Differential fates of biomolecules delivered to target cells via extracellular vesicles. Proc Natl Acad Sci U S A. 2015;112:E1433–42. [PubMed: 25713383]
21. Mohamed TMA, Ang YS, Radzinsky E, Zhou P, Huang Y, Elfenbein A, Foley A, Magnitsky S and Srivastava D. Regulation of Cell Cycle to Stimulate Adult Cardiomyocyte Proliferation and Cardiac Regeneration. Cell. 2018;173:104–116 e12. [PubMed: 29502971]
22. Tian Y, Liu Y, Wang T, Zhou N, Kong J, Chen L, Snitow M, Morley M, Li D, Petrenko N, Zhou S, Lu M, Gao E, Koch WJ, Stewart KM and Morrisey EE. A microRNA-Hippo pathway that promotes cardiomyocyte proliferation and cardiac regeneration in mice. Sci Transl Med. 2015;7:279ra38.
23. Torrini C, Cubero RJ, Dirkx E, Braga L, Ali H, Prosdocimo G, Gutierrez MI, Collesi C, Licastro D, Zentilin L, Mano M, Zacchigna S, Vendruscolo M, Marsili M, Samal A and Giacca M. Common Regulatory Pathways Mediate Activity of MicroRNAs Inducing Cardiomyocyte Proliferation. Cell Rep. 2019;27:2759–2771 e5. [PubMed: 31141697]
24. Hong W and Guan KL. The YAP and TAZ transcription co-activators: key downstream effectors of the mammalian Hippo pathway. Semin Cell Dev Biol. 2012;23:785–93. [PubMed: 22659496]
25. Krishnan A, Samtani R, Dhanantwari P, Lee E, Yamada S, Shiota K, Donofrio MT, Leatherbury L and Lo CW. A detailed comparison of mouse and human cardiac development. Pediatr Res. 2014;76:500–7. [PubMed: 25167202]
26. Chong JJ, Yang X, Don CW, Minami E, Liu YW, Weyers JJ, Mahoney WM, Van Biber B, Cook SM, Palpant NJ, Gantz JA, Fugate JA, Muskheli V, Gough GM, Vogel KW, Astley CA, Hotchkiss

CE, Baldessari A, Pabon L, Reinecke H, Gill EA, Nelson V, Kiem HP, Laflamme MA and Murry CE. Human embryonic-stem-cell-derived cardiomyocytes regenerate non-human primate hearts. Nature. 2014;510:273–7. [PubMed: 24776797]

27. Liu YW, Chen B, Yang X, Fugate JA, Kalucki FA, Futakuchi-Tsuchida A, Couture L, Vogel KW, Astley CA, Baldessari A, Ogle J, Don CW, Steinberg ZL, Seslar SP, Tuck SA, Tsuchida H, Naumova AV, Dupras SK, Lyu MS, Lee J, Hailey DW, Reinecke H, Pabon L, Fryer BH, MacLellan WR, Thies RS and Murry CE. Human embryonic stem cell-derived cardiomyocytes restore function in infarcted hearts of non-human primates. Nat Biotechnol. 2018;36:597–605. [PubMed: 29969440]
28. Tachibana A, Santoso MR, Mahmoudi M, Shukla P, Wang L, Bennett M, Goldstone AB, Wang M, Fukushi M, Ebert AD, Woo YJ, Rulifson E and Yang PC. Paracrine Effects of the Pluripotent Stem Cell-Derived Cardiac Myocytes Salvage the Injured Myocardium. Circ Res. 2017;121:e22–e36. [PubMed: 28743804]
29. White HD, Norris RM, Brown MA, Brandt PW, Whitlock RM and Wild CJ. Left ventricular end-systolic volume as the major determinant of survival after recovery from myocardial infarction. Circulation. 1987;76:44–51. [PubMed: 3594774]
30. Dai Z, Aoki T, Fukumoto Y and Shimokawa H. Coronary perivascular fibrosis is associated with impairment of coronary blood flow in patients with non-ischemic heart failure. J Cardiol. 2012;60:416–21. [PubMed: 22867802]
31. Gnecchi M, He H, Noiseux N, Liang OD, Zhang L, Morello F, Mu H, Melo LG, Pratt RE, Ingwall JS and Dzau VJ. Evidence supporting paracrine hypothesis for Akt-modified mesenchymal stem cell-mediated cardiac protection and functional improvement. FASEB J. 2006;20:661–9. [PubMed: 16581974]
32. Dai W, Wold LE, Dow JS and Kloner RA. Thickening of the infarcted wall by collagen injection improves left ventricular function in rats: a novel approach to preserve cardiac function after myocardial infarction. J Am Coll Cardiol. 2005;46:714–9. [PubMed: 16098441]
33. Duran JM, Taghavi S, Berretta RM, Makarewich CA, Sharp Iii T, Starosta T, Udeshi F, George JC, Kubo H and Houser SR. A characterization and targeting of the infarct border zone in a swine model of myocardial infarction. Clin Transl Sci. 2012;5:416–21. [PubMed: 23067355]
34. Miyagawa S, Sawa Y, Taketani S, Kawaguchi N, Nakamura T, Matsuura N and Matsuda H. Myocardial regeneration therapy for heart failure: hepatocyte growth factor enhances the effect of cellular cardiomyoplasty. Circulation. 2002;105:2556–61. [PubMed: 12034665]
35. Shiojima I, Sato K, Izumiya Y, Schiekofer S, Ito M, Liao R, Colucci WS and Walsh K. Disruption of coordinated cardiac hypertrophy and angiogenesis contributes to the transition to heart failure. J Clin Invest. 2005;115:2108–18. [PubMed: 16075055]
36. Winegrad S, Henrion D, Rappaport L and Samuel JL. Vascular endothelial cell-cardiac myocyte crosstalk in achieving a balance between energy supply and energy use. Adv Exp Med Biol. 1998;453:507–14. [PubMed: 9889863]
37. Valadi H, Ekstrom K, Bossios A, Sjostrand M, Lee JJ and Lotvall JO. Exosome-mediated transfer of mRNAs and microRNAs is a novel mechanism of genetic exchange between cells. Nat Cell Biol. 2007;9:654–9. [PubMed: 17486113]
38. Tseliou E, Fouad J, Reich H, Slipczuk L, de Couto G, Aminzadeh M, Middleton R, Valle J, Weixin L and Marban E. Fibroblasts Rendered Antifibrotic, Antiapoptotic, and Angiogenic by Priming With Cardiosphere-Derived Extracellular Membrane Vesicles. J Am Coll Cardiol. 2015;66:599–611. [PubMed: 26248985]
39. Sun X, Dai G, Yu L, Hu Q, Chen J and Guo W. miR-143–3p inhibits the proliferation, migration and invasion in osteosarcoma by targeting FOSL2. Sci Rep. 2018;8:606. [PubMed: 29330462]
40. Wen SY, Lin Y, Yu YQ, Cao SJ, Zhang R, Yang XM, Li J, Zhang YL, Wang YH, Ma MZ, Sun WW, Lou XL, Wang JH, Teng YC and Zhang ZG. miR-506 acts as a tumor suppressor by directly targeting the hedgehog pathway transcription factor Gli3 in human cervical cancer. Oncogene. 2015;34:717–25. [PubMed: 24608427]
41. Stanley-Hasnain S, Hauck L, Grothe D, Aschar-Sobbi R, Beca S, Butany J, Backx PH, Mak TW and Billia F. p53 and Mdm2 act synergistically to maintain cardiac homeostasis and mediate cardiomyocyte cell cycle arrest through a network of microRNAs. Cell Cycle. 2017;16:1585–1600. [PubMed: 28745540]

42. Huang W, Feng Y, Liang J, Yu H, Wang C, Wang B, Wang M, Jiang L, Meng W, Cai W, Medvedovic M, Chen J, Paul C, Davidson WS, Sadayappan S, Stambrook PJ, Yu XY and Wang Y. Loss of microRNA-128 promotes cardiomyocyte proliferation and heart regeneration. Nat Commun. 2018;9:700. [PubMed: 29453456]
43. Gabisonia K, Prosdocimo G, Aquaro GD, Carlucci L, Zentilin L, Secco I, Ali H, Braga L, Gorgodze N, Bernini F, Burchielli S, Collesi C, Zandona L, Sinagra G, Piacenti M, Zacchigna S, Bussani R, Recchia FA and Giacca M. MicroRNA therapy stimulates uncontrolled cardiac repair after myocardial infarction in pigs. Nature. 2019;569:418–422. [PubMed: 31068698]
44. Ye L, Chang YH, Xiong Q, Zhang P, Zhang L, Somasundaram P, Lepley M, Swingen C, Su L, Wendel JS, Guo J, Jang A, Rosenbush D, Greder L, Dutton JR, Zhang J, Kamp TJ, Kaufman DS, Ge Y and Zhang J. Cardiac repair in a porcine model of acute myocardial infarction with human induced pluripotent stem cell-derived cardiovascular cells. Cell Stem Cell. 2014;15:750–61. [PubMed: 25479750]
45. Rikkert LG, Nieuwland R, Terstappen L and Coumans FAW. Quality of extracellular vesicle images by transmission electron microscopy is operator and protocol dependent. J Extracell Vesicles. 2019;8:1555419. [PubMed: 30651939]
46. Guo GR, Chen L, Rao M, Chen K, Song JP and Hu SS. A modified method for isolation of human cardiomyocytes to model cardiac diseases. J Transl Med. 2018;16:288. [PubMed: 30348184]
47. Eulalio A, Mano M, Dal Ferro M, Zentilin L, Sinagra G, Zacchigna S and Giacca M. Functional screening identifies miRNAs inducing cardiac regeneration. Nature. 2012;492:376–81. [PubMed: 23222520]
48. Zhang J, Klos M, Wilson GF, Herman AM, Lian X, Raval KK, Barron MR, Hou L, Soerens AG, Yu J, Palecek SP, Lyons GE, Thomson JA, Herron TJ, Jalife J and Kamp TJ. Extracellular matrix promotes highly efficient cardiac differentiation of human pluripotent stem cells: the matrix sandwich method. Circulation research. 2012;111:1125–36. [PubMed: 22912385]
49. Zhu W, Zhao M, Mattapally S, Chen S and Zhang J. CCND2 Overexpression Enhances the Regenerative Potency of Human Induced Pluripotent Stem Cell-Derived Cardiomyocytes: Remuscularization of Injured Ventricle. Circulation research. 2018;122:88–96. [PubMed: 29018036]

Clinical Perspective

What is new?

- It is first time to validate the enhanced potency of hiPSC-MHC-CCND2^{OE}CMs in prompting myocyte proliferation of AMI hearts in a preclinical large-animal model.
- The CCND2^{OE}CMs transplantation associated with promoting the proliferation of recipient heart CMs, ECs, and SMCs at least partly by paracrine activity.
- hiPSC-CMs and rodent cardiomyocytes exhibited higher proliferative activity upon co-culture with the Exosome released from the CCND2^{OE} or miR-373-302b mimic compared to culture with exosome from the CCND2^{WT} or control miRNA mimics.

What Are the Clinical Implications?

- Enhanced proliferative capability of cardiomyocytes allowed lowering of the initial administration dose of the CMs
- Promote a novel therapeutic strategy aiming at upregulating proliferation of the recipient cardiac cells using hiPSC derived cell or cell products.
- Targeting the myocyte cell-cycle regulators such as CCND2 holds a strategic potential for remuscularization of myocardial infarct.

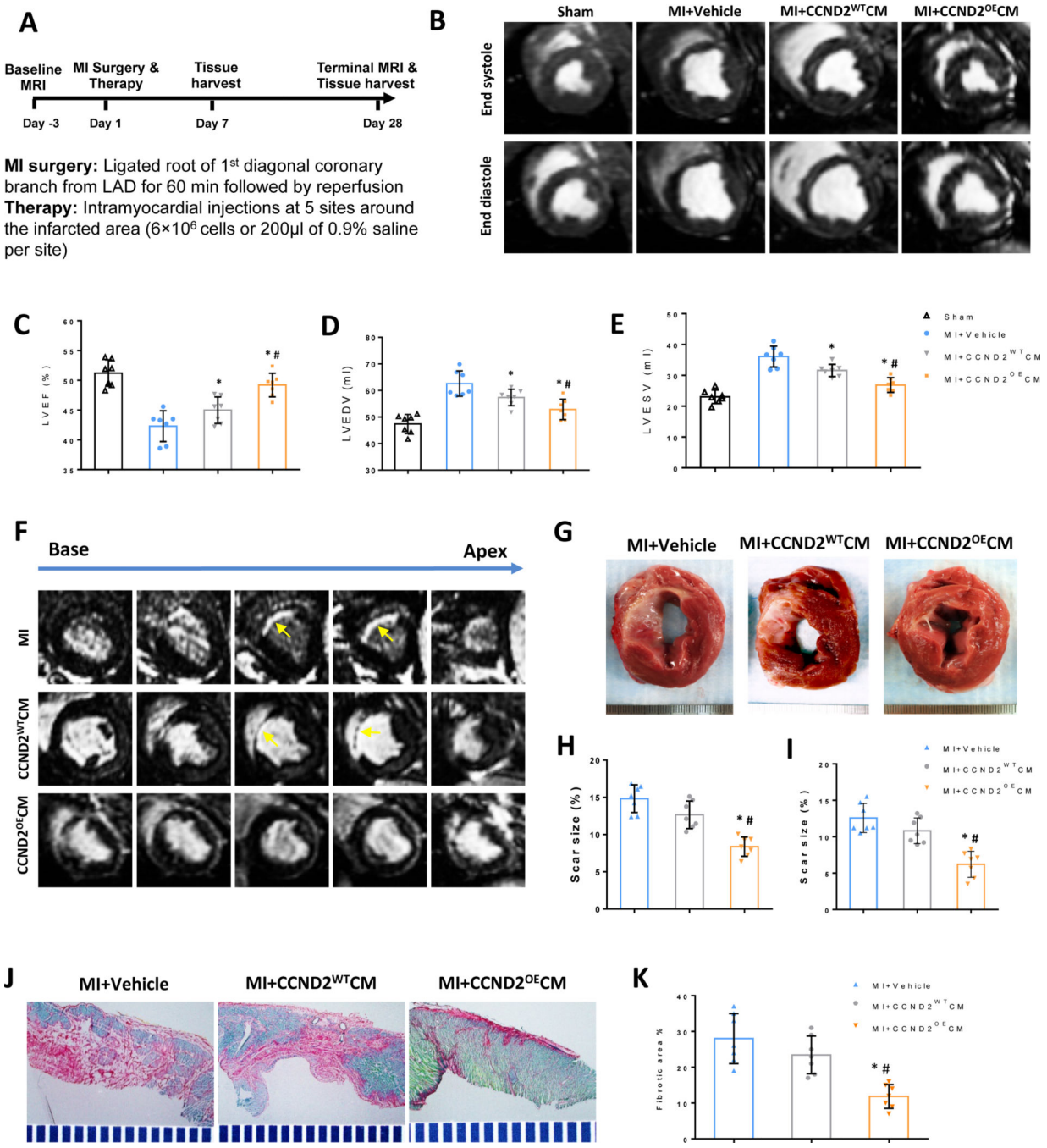

Figure 1. CCND2^{OE}CMs show greater potency than CCND2^{WT}CMs for recovery from MI in swine.

(A) The study design schematic. MI was surgically induced in pigs via a 60-minute ligation of the LAD coronary artery. After reperfusion, animals in the MI+CCND2^{OE}CM group were treated with CCND2-overexpressing hiPSC-CMs, animals in the MI+CCND2^{WT}CM group were treated with hiPSC-CMs that expressed wild type (“normal”) levels of CCND2, and animals in the MI+Vehicle group were treated with the delivery vehicle alone; animals in the SHAM group underwent the same surgical procedures for MI induction except LAD coronary artery ligation and recovered without any of the experimental treatments. Four

weeks after MI induction cMRI was performed, and the images (B) were used to calculate left-ventricular ejection fraction (LVEF) (C), end-diastolic volume (LVEDV) (D), end-systolic volume (LVESV) (E), cMRI images of base-to-apex cross-sections of the representative porcine hearts at 4 weeks after receiving MI+vehicle, MI+CCND2^{WT}CMs or MI+CCND2^{OE}CMs treatments (F). A representative porcine MI heart cross-section at 4 weeks after receiving the vehicle only, the CCND2^{WT}CMs or the CCND2^{OE}CMs injection treatment. Scar-sizes in the cross-sections were evaluated via a cMRI (H) or histological assessments in fresh tissue sections (I) and presented as a percentage of the total LV surface area (G). Fibrosis was evaluated in sections stained with Sirius Red (fibrotic tissue) and Fast Green (functional cardiac tissue) (J) and quantified as a ratio of the fibrotic area to the sum of the fibrotic and non-fibrotic areas, and presented as a percentage (K); * $p<0.05$ relative to MI+Vehicle control; # $p<0.05$ relative to MI+CCND2^{WT}CM.

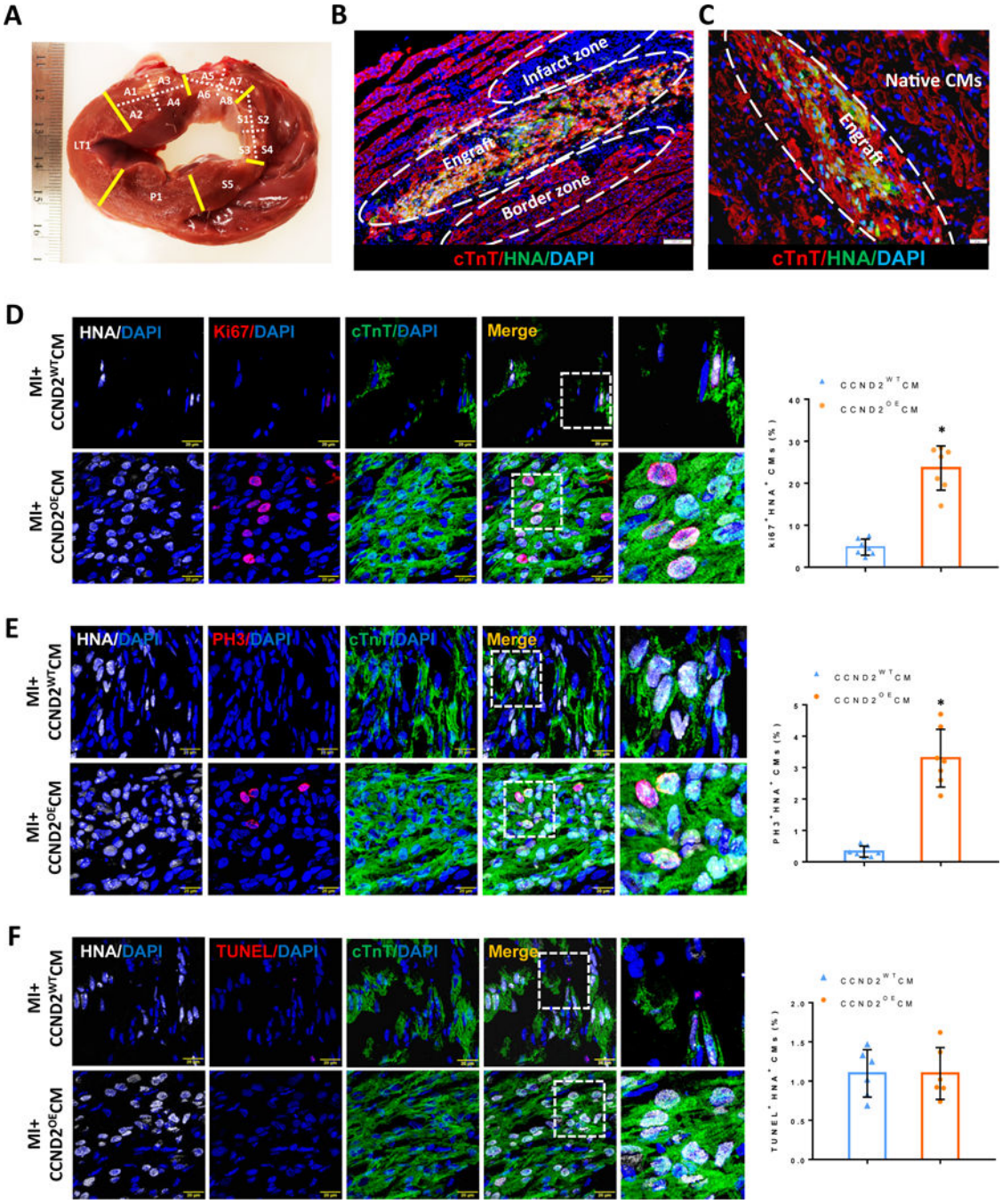

Figure 2. CCND2^{OE}CMs proliferated after transplantation into infarcted pig hearts.

(A) Gross anatomy of a single cardiac slice from a porcine heart at 4 weeks after the surgery: each slice was divided into different sub-regions for Y-chromosome quantification and other analyses. (B and C) Immunofluorescence images of tissue sections of the porcine hearts subjected to myocardial infarction and transplantation of CCND2^{OE}CMs 4 weeks after the treatment. The transplanted hiPSC-CMs were identified by co-expression of cTnT (red) and HNA (green). The Infarct zone, the border zone, the graft and the native (recipient) CMs in the infarcted porcine hearts are marked inside the white dashed ovals or simply

marked (Native CMs) on the image panels (B and C), respectively. The scale bars are 100 μm and 20 μm. (D-F) Sections from the infarct border zone were stained for HNA to identify CMs of the human origin (hiPSC-CMs), for cTnT to verify CM identity, for Ki67 (D) and phosphorylated histone 3 (PH3) (E) to verify proliferating activity of the CMs. TUNEL staining was performed to assess the level of apoptosis in the CMs (F). Nuclei were counter-stained with DAPI, and hiPSC-CM proliferation was quantified and presented as a percentage of HNA-expressing cells that also expressed Ki67 or PH3; hiPSC-CM apoptosis was quantified as a percentage of the HNA-expressing cells positive for TUNEL staining. The scale bar is 20 μm; * $p<0.05$ relative to MI+CCND2^{WT}CM.

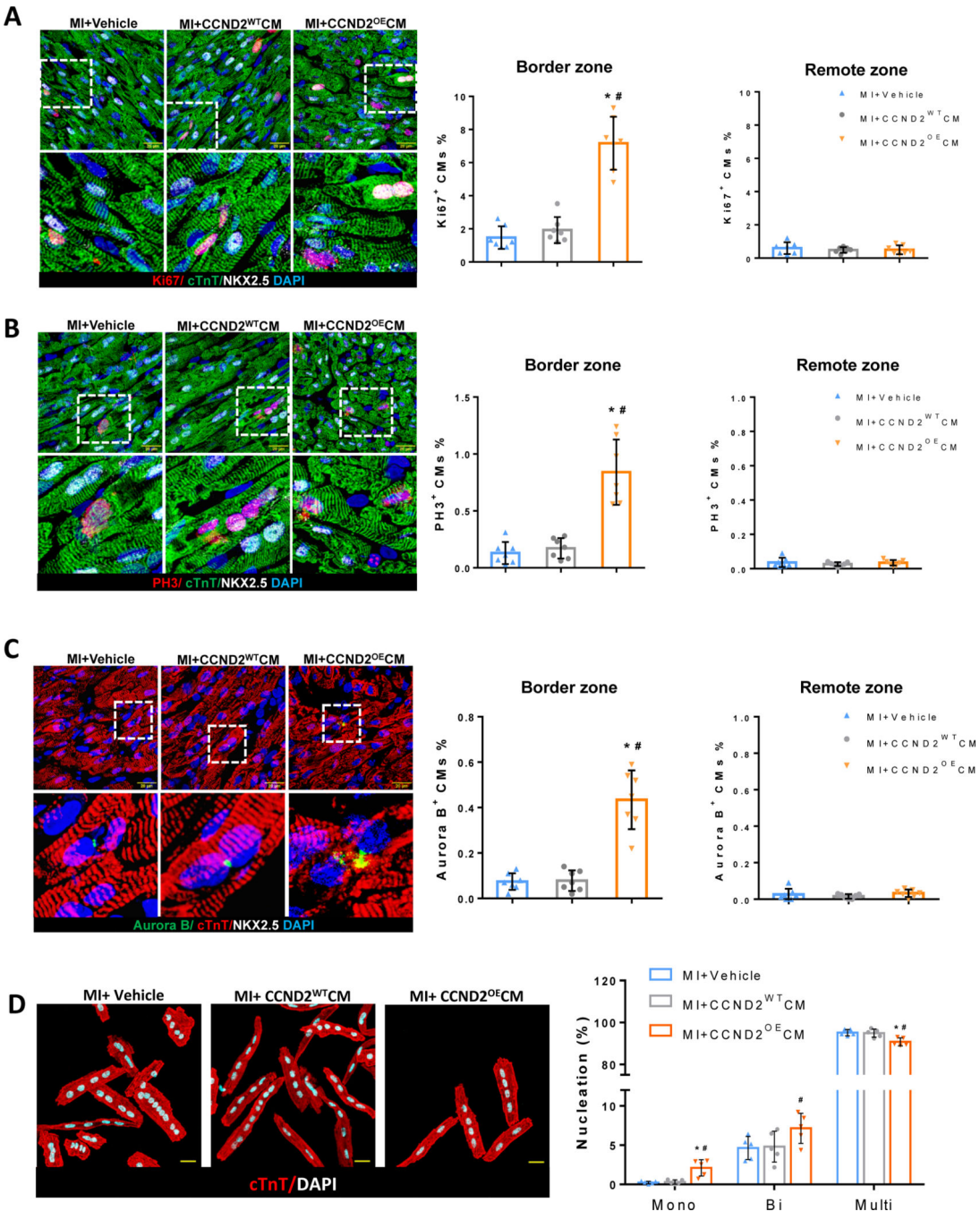

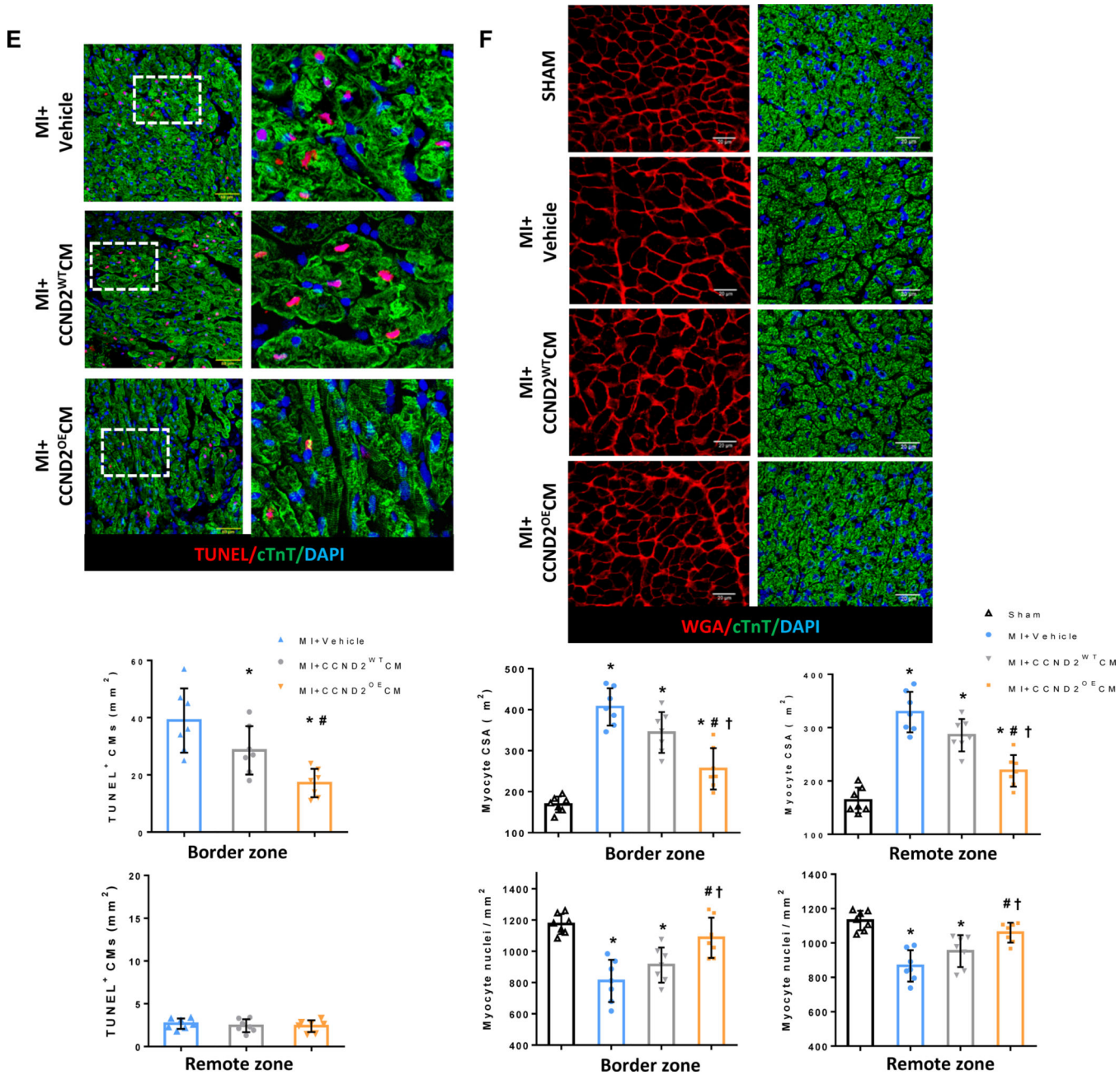

Figure 3. Endogenous CMs were more proliferative and resistant to MI-induced apoptosis and hypertrophy in CCND2^{OE}CM-treated than in CCND2^{WT}CM-treated animals.

(A-C and E-F) Sections from the BZ and RZ were stained for cTnT to visualize all CMs, for (A-C) the transcription factor Nkx2.5, which represents the cardiomyocyte nucleus, for the proliferation markers (A) Ki67, (B) PH3, and (C) Aurora B. Representative images of immunofluorescent staining (A-C) are shown for the BZ only. Nuclei were counterstained with DAPI, and then endogenous CM proliferation was quantified as the percentage of cTNT-expressing cells with the proliferation markers. (D) Representative images of dissociated single cardiomyocytes from the BZ of porcine hearts at 4 weeks after surgery. Moreover, quantification of the percentage of CMs was exhibiting different nucleation. The

experiment was performed in a single-blind manner and a minimal of 1000 CMs from each group was counted. (E) Representative images of TUNEL staining and endogenous CM apoptosis were quantified as the percentage of cTnT-expressing cells with TUNEL positive cells. (F) Sections from the BZ and RZ were stained for cTnT to visualize CMs with wheat germ agglutinin (WGA) to visualize cell borders. Nuclei were counterstained with DAPI, and then cell size was quantified via measurements of CM cross-sectional surface area (CSA), and the density of CM nuclei was calculated. The scale bar=20 μm. Panels A-E: *P<0.05 vs. MI+Vehicle, #P<0.05 vs. MI+CCND2^{WT}CM; panel F: *P<0.05 vs. SHAM, $^{\#}$P<0.05 vs. MI+Vehicle, †P<0.05 vs. MI+CCND2^{WT}CM.

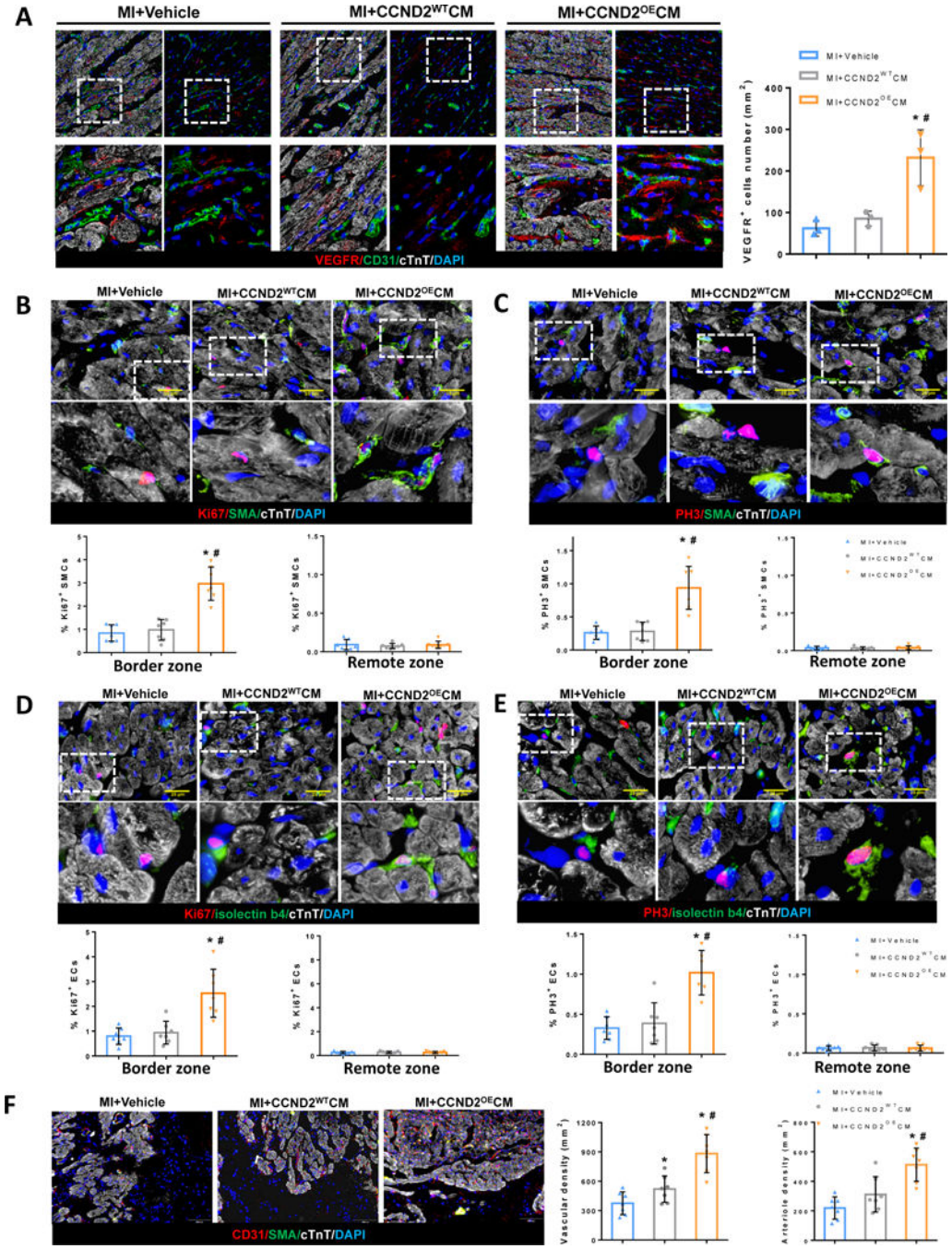

Figure 4. Angiogenic activity in the infarcted porcine hearts was greater following their treatment with CCND2^{OE}CMs than with CCND2^{WT}CMs.

(A) Representative images of immunofluorescence tissue staining for VEGFR and quantification of VEGFR^{+} cells from the BZ of the porcine hearts at 1 week after surgery. Sections from the BZ and the RZ were stained for cTnT to visualize/identify all CMs (A-E), for the proliferation markers Ki67 (B and D), PH3 (C and E), and for smooth-muscle actin (SMA) to identify smooth-muscle cells (SMCs) (B and C) or for CD31(A) or isolectin B4 (D and E) to identify endothelial cells (ECs). Nuclei were counterstained with DAPI, and proliferation of SMCs was quantified as a percentage of SMA^{+} also expressing Ki67 or PH3

(B, C bar graphs, respectively); Correspondingly, the proliferation of ECs was quantified as a percentage of isolectin-B4^{+} cells also positive for Ki67 or PH3 (D, E bar graphs, respectively). (F) BZ and RZ sections of the MI hearts stained for the endothelial marker CD31 and costained for cTnT and SMA; Nuclei were counterstained with DAPI. Arteriole and capillary densities were quantified as a number of SMA^{+} and CD31^{+} structures per area unit. * $p<0.05$ relative to MI+Vehicle, $^{\#}$ $p<0.05$ relative to MI+CCND2^{WT}CM.

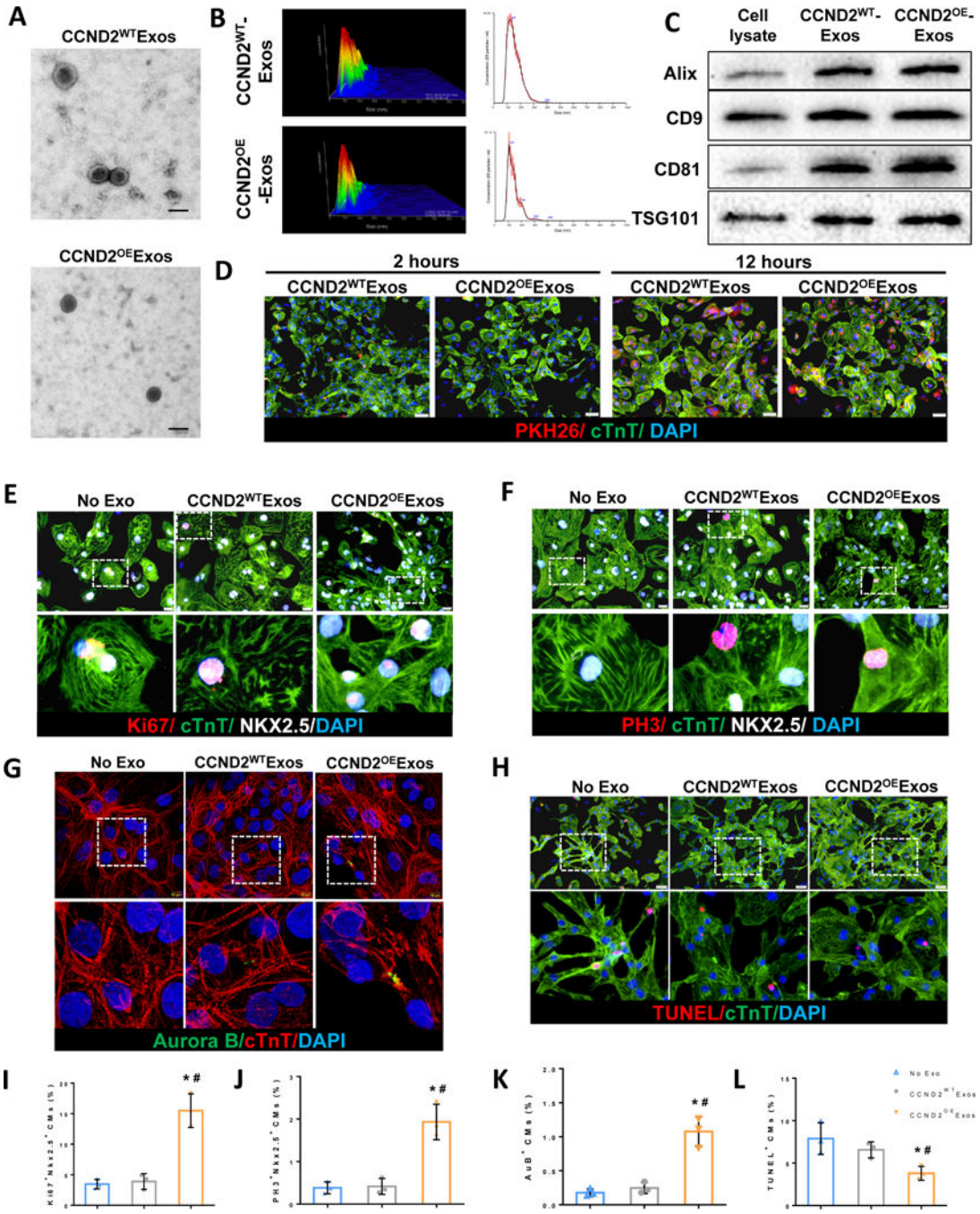

Figure 5. hiPSC-CMs were more proliferative and more resistant to hypoxia-induced apoptosis when cultured with exosomes from CCND2^{OE}CMs than exosomes from CCND2^{WT}CMs.

Exosomes were isolated from the culture medium of CCND2^{OE}CMs (CCND2^{OE}Exos) and CCND2^{WT}CMs (CCND2^{WT}Exos). (A) Electron microscopy analysis of exosomes produced from CCND2^{WT}CMs and CCND2^{OE}CMs. The scale bar=100 nm. (B) The distribution of exosome sizes was evaluated via nanoparticle-tracking analysis. Moreover, (C) the presence of exosomal marker proteins Alix, CD9, CD81, and TSG101 was confirmed via Western blot. (D) hiPSC-CMs were cultured with exosomes that had been fluorescently labeled with PKH26 for 2 hrs or 12 hrs, followed by fixing and staining for cTnT. Nuclei were

counterstained with DAPI. Cellular uptake of the exosomes was confirmed via assessments of PKH26 fluorescence. (E-G) hiPSC-CMs were cultured with $CCND2^{OE}$Exos, $CCND2^{WT}$Exos, or phosphate-buffered saline (PBS) under normoxic conditions for 72 hrs, followed by fixing and staining for cTnT, and the proliferation markers (E) Ki67, (F) PH3, or (G) Aurora B. Nuclei were counterstained with DAPI, and hiPSC-CM proliferation was quantified as the percentage of cells that expressed each of the proliferation markers (I-K). (H) hiPSC-CMs were cultured with adding $CCND2^{OE}$Exos, $CCND2^{WT}$Exos, or PBS under hypoxic conditions for 48 hrs, fixed, and stained for cTnT and TUNEL. Nuclei were counterstained with DAPI. hiPSC-CM apoptosis was quantified as the percentage of cells that were $TUNEL^{+}$ (L).*$P<0.05$ vs. PBS, $^{\#}P<0.05$ vs. $CCND2^{WT}$Exo. Each experiment was performed independently for 3 times.

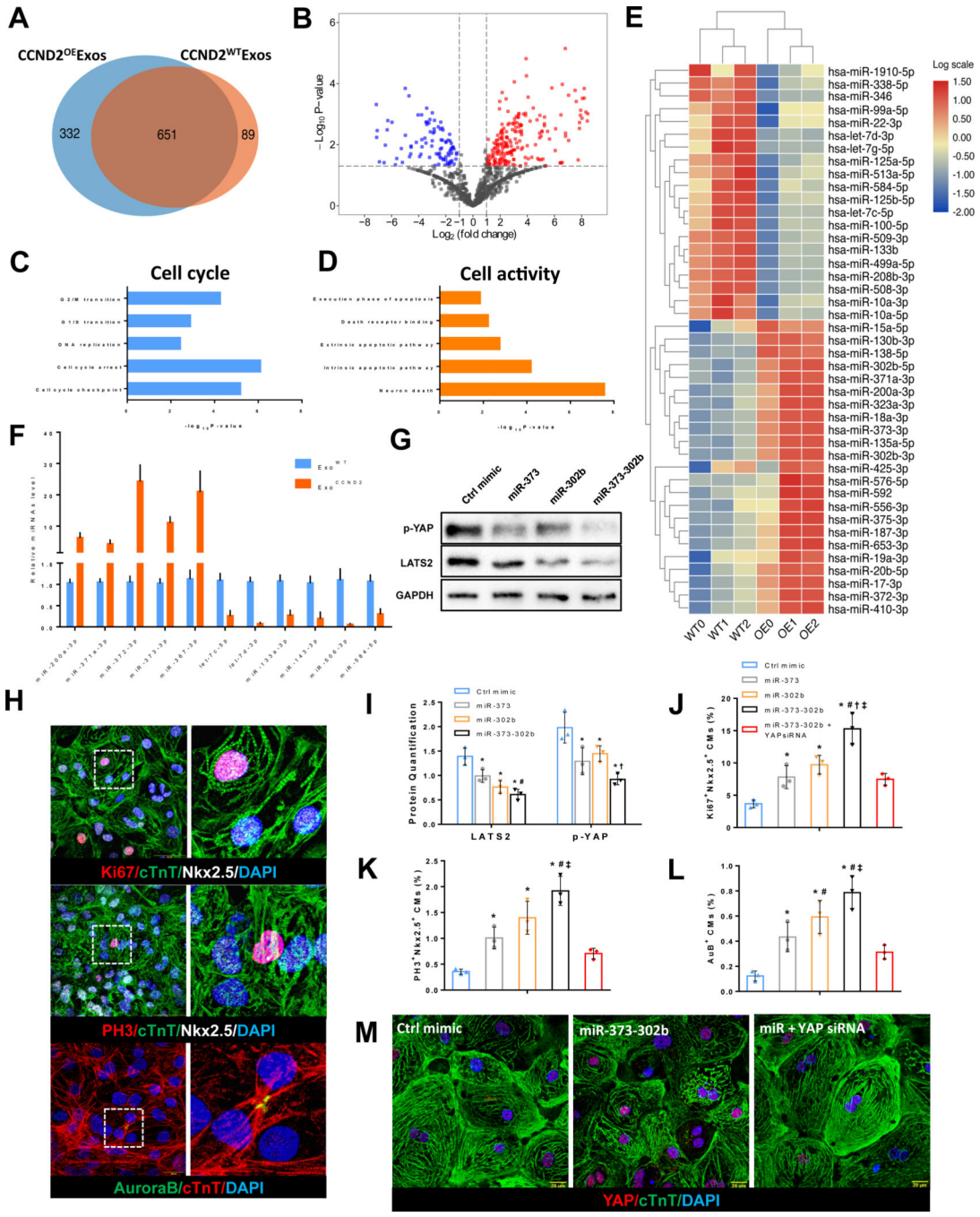

Figure 6. CCND2 overexpression in the hiPSC-CMs alters the miRNA content of the hiPSC-CM-secreted exosomes.

(A-E) Identification of miRNA content of the CCND2^{WT}Exos and the CCND2^{OE}Exos by a bulk miRNA sequence analysis. (A) A Venn diagram depicting the identified exosome-derived miRNAs specific and common for each of the exosome populations (CCND2^{WT}Exos and CCND2^{OE}Exos), (B) miRNAs that are present in both CCND2^{WT}Exos and CCND2^{OE}Exos are shown as a volcano plot; the common miRNAs that were present in both exosomal populations in comparable quantities are depicted as gray dots, while the exosomes that were significantly up- or down-regulated in CCND2^{OE}Exos

are depicted with red or blue dots, respectively. (C and D) Gene Ontology analysis was performed to reveal significant differences between the $CCND2^{WT}$Exo and the $CCND2^{OE}$Exo populations in miRNAs of the cell cycle (C) or the cell death (D) functional categories. (E) The cell-cycle associated miRNAs with significantly different expression levels are depicted in the heat map of Panel 6E. (F) The expression of miRNAs implicated in regulation of cell proliferation (miR-200a-3p, miR-371a-3p, miR-372-3p, miR-373-3p, miR-367-3p) and apoptosis (let-7c-5p, let-7d-3p, miR-133a-3p, miR-143-3p, miR-506-3p, miR-584-5p) was quantified in the $CCND2^{WT}$Exo and the $CCND2^{OE}$Exo populations by qRT-PCR. (G-L) The effect of individual miRNA overexpression recapitulated by transfection of the $CCND2^{WT}$-CMs with Ctrl-mimic, miR-373-3p mimic, miR-302b-3p mimic, miR-373-302b mimic or miR-373-302b mimic+YAP siRNA analyzed 72 hrs post-transfection. The expression levels of p-YAP and LATS2 upon transient overexpression of various miRNAs were analyzed by western blot (G) and quantified by densitometry, following normalization by GAPDH (I). The effect of the miRNAs on the CM proliferation was assessed by immunofluorescence analyses of Ki67, PH3, and Aurora B expression (H) and quantified as a percentage of cTNT-expressing cells that also expressed Ki67 (J), PH3 (K), or Aurora B (AuB) (L). Right column images in panel H represent insets/blow-up images for the boxed areas. (M) Representative images for an immunofluorescence staining for YAP (red) and cTnT (green) in the hiPSC-CMs transfected with Ctrl mimic, miR-373-302b mimic, or miR-373-302b mimic+YAP siRNA, performed 72 hrs post-transfection. The scale bar is 20 μm. * $p<0.05$ relative to Ctrl mimic, $^{\#}$ $p<0.05$ relative to miR-373 mimic, † $p<0.05$ relative to miR-302b mimic, ‡ $p<0.05$ relative to miR-302b-373 mimic+YAP siRNA.

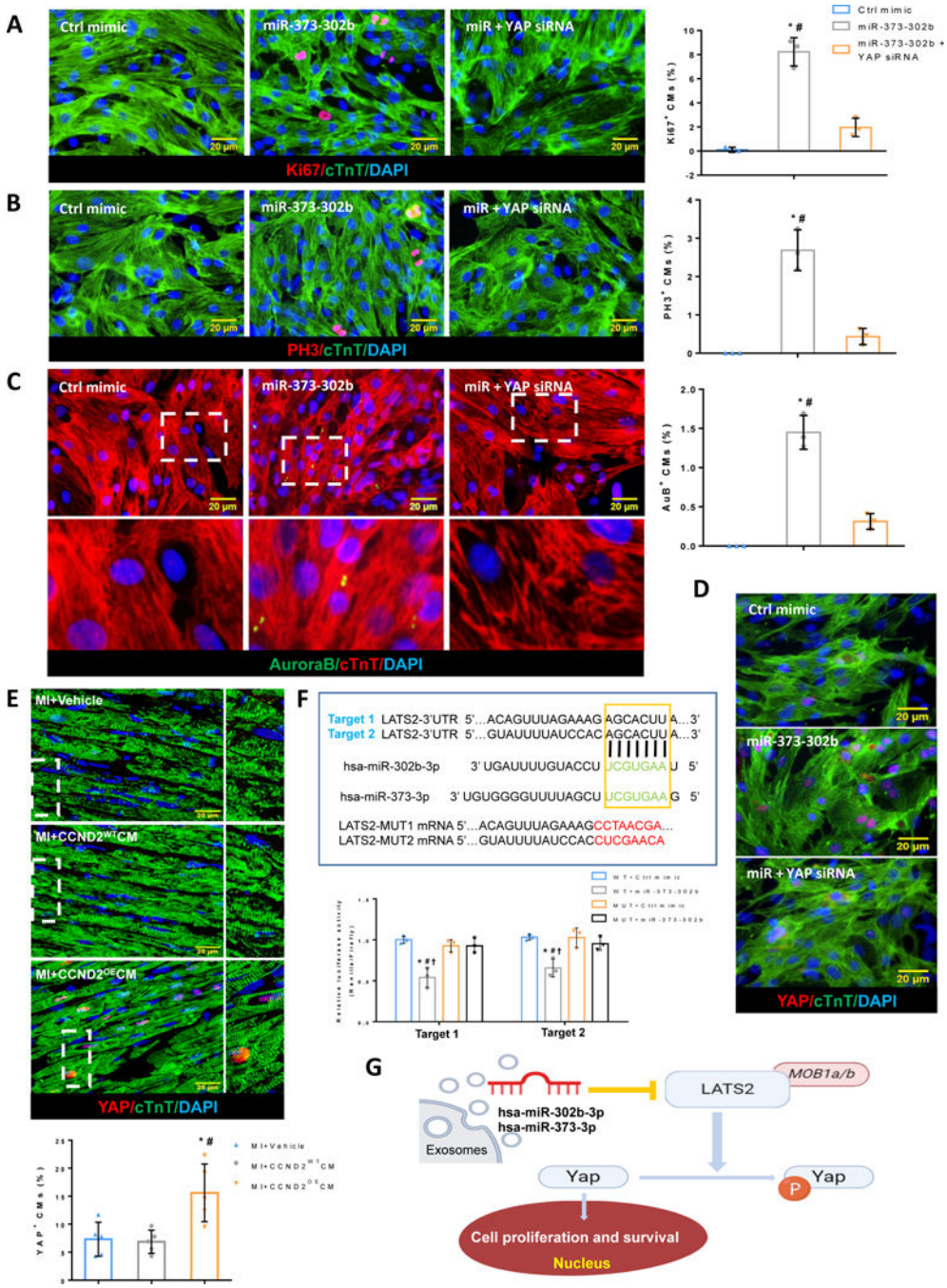

Figure 7. miR-302b-373 induces cardiomyocyte proliferation by regulation of the Hippo signaling pathway.

(A-C) Immunofluorescence microscopy images of the tracked primary rat cardiomyocytes expressing (A) proliferation marker Ki67 (red), (B) cell cycle M-phase marker PH3 (red), and (C) cytokinesis marker Aurora B kinase (green), captured 72 hrs after transfection with Ctrl mimic, miR-373-302b mimic or miR-373-302b mimic + YAP siRNA. Cell cycle activity in the CMs was analyzed by quantification of $Ki67^+$, $PH3^+$, or Aurora B^+ CMs as a percentage of total $cTnT^+$ CMs (A-C bar graphs, respectively). Nuclei were stained with DAPI (blue). The scale bar is 20 μm. * $p<0.05$ relative to Ctrl mimic, # $p<0.05$ relative to

miR-373-302b mimic+YAP siRNA. (D) Representative immunofluorescence images of the tracked primary rat cardiomyocytes expressing YAP (red) 72 hrs after transfection with Ctrl mimic, miR-373-302b mimic or miR-373-302b mimic+YAP siRNA. The scale bar is 20 μm. (E) Representative confocal microscopy images and quantification of the swine CMs with YAP nuclei translocation (E bar graph) in the heart BZs 4 weeks after the hiPSC-CMs transplantation. Smaller (right column) images in panel E represent insets/blow-up images for the boxed areas. The scale bar is 20 μm. * $p<0.05$ relative to MI only, # $p<0.05$ relative to MI+CCND2^{WT} CMs. (F) Validation of the miRNA binding effect to their predicted LATS2 miRNA-target by a dual-luciferase reporter assay. Two putative target sites for hsa-miR-302b-3p were predicted by the TargetScan server in the 3'UTR of the LATS2 mRNA (highlighted in the boxed area). The mutated target sequences are shown below. Relative luciferase activity was measured 48 hrs after co-transfection with luciferase reporters carrying the wild-type or the mutated 3'UTRs of LATS2, as well as the miR-302b mimic or Ctrl mimic in HEK293 cells (F bar graph). WT- wild type, MT- Mutation site. * $p<0.05$ relative to WT+Ctrl mimic, # $p<0.05$ relative to MT+Ctrl mimic, † $p<0.05$ relative to MT +miR-302b mimic. (G) The general view of how miR-302b-3p and miR-373-3p work on the Hippo pathway through inhibiting LATS2, thus causing cell proliferation and survival.